

pubs.acs.org/jmc Article

# Physachenolide C is a Potent, Selective BET Inhibitor

Christopher J. Zerio,<sup>†</sup> Jared Sivinski,<sup>†</sup> E. M. Kithsiri Wijeratne, Ya-Ming Xu, Duc T. Ngo, Andrew J. Ambrose, Luis Villa-Celis, Niloofar Ghadirian, Michael W. Clarkson, Donna D. Zhang, Nancy C. Horton, A. A. Leslie Gunatilaka,\* Raimund Fromme,\* and Eli Chapman\*



Cite This: https://doi.org/10.1021/acs.jmedchem.2c01770



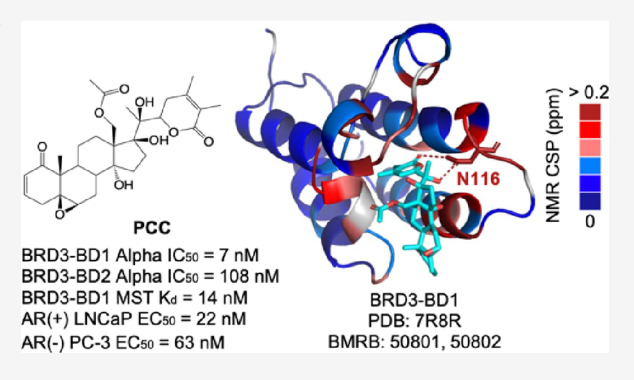
**ACCESS** 

III Metrics & More

Article Recommendations

s Supporting Information

**ABSTRACT:** A pulldown using a biotinylated natural product of interest in the  $17\beta$ -hydroxywithanolide (17-BHW) class, physachenolide C (PCC), identified the bromodomain and extra-terminal domain (BET) family of proteins (BRD2, BRD3, and BRD4), readers of acetyllysine modifications and regulators of gene transcription, as potential cellular targets. BROMOscan bromodomain profiling and biochemical assays support PCC as a BET inhibitor with increased selectivity for bromodomain (BD)-1 of BRD3 and BRD4, and X-ray crystallography and NMR studies uncovered specific contacts that underlie the potency and selectivity of PCC toward BRD3-BD1 over BRD3-BD2. PCC also displays characteristics of a molecular glue, facilitating proteasome-mediated degradation of BRD3 and BRD4. Finally, PCC is more potent than other withanolide analogues and gold-standard pan-BET inhibitor



(+)-JQ1 in cytotoxicity assays across five prostate cancer (PC) cell lines regardless of androgen receptor (AR)-signaling status.

## **■** INTRODUCTION

Prostate cancer (PC) is the second most common cancer among men in the United States, and one in eight men will be diagnosed with PC in their lifetime.<sup>2</sup> PC research has focused on the androgen receptor (AR), which predominantly drives the disease, and multiple drugs that reduce AR signaling have been clinically approved. Namely, abiraterone acts as a potent antagonist of androgen synthesis, and enzalutamide blocks androgen binding to AR.3 Although both of these drugs are initially effective and enhance survival of PC patients, androgen deprivation therapy (ADT) loses efficacy due to the development of castration-resistant prostate cancer (CRPC), a disease state that features reactivation of AR signaling and a rise in ARregulated prostate-specific antigen (PSA).<sup>4</sup> In some instances, ADT results in the production of drug-resistant AR splice variants, AR copy number amplification, or increased dependency on other oncogenic signaling pathways.<sup>7</sup> This transformation can generate CRPCs that do not express AR (AR-negative) and are reliant on survival mechanisms completely distinct from those regulated by AR signaling.<sup>8,9</sup> This observation has promoted new efforts to target ARnegative CRPCs that operate independently of AR signaling. Additionally, ADT drug resistance has provoked investment in treatments that target AR differently, possibly through inhibition of co-activators that support the transcriptional activity of AR. 10,11

Histone acetylation is a post-translational modification that blocks the ionic interaction between the positively charged histone core and the negatively charged DNA backbone. This structural interruption opens the chromatin, increases access by polymerases and transcription factors, and activates gene expression. Histone acetylation levels are tightly regulated not only by histone acetyltransferases and histone deacetylases but also by a family of epigenetic reader proteins called bromodomain-containing proteins, which specifically recognize N-acetylation of lysine residues  $(K_{ac})^{12}$ . The human proteome encodes 61 bromodomains (BDs) present in 46 nuclear and cytoplasmic proteins<sup>13</sup> broken up into eight groups based on their structural properties. 14 Group two includes the bromodomain and extra-terminal domain (BET) family of proteins. Despite the widespread nature of BET protein substrates and their broad roles in transcriptional elongation, it was discovered that inhibition of BET proteins prevents detection of protranscription markers and selectively interferes with the transcription of a relatively small number of gene networks. 13 These networks include genes involved in the inflammatory response in immune  $\operatorname{cells}^{15}$  as well as cellular growth and evasion of apoptosis in cancer. 16-18 As a result, BET proteins have become pharmaceutical targets as BET inhibitors may be able to

Received: October 31, 2022



**Journal of Medicinal Chemistry** 

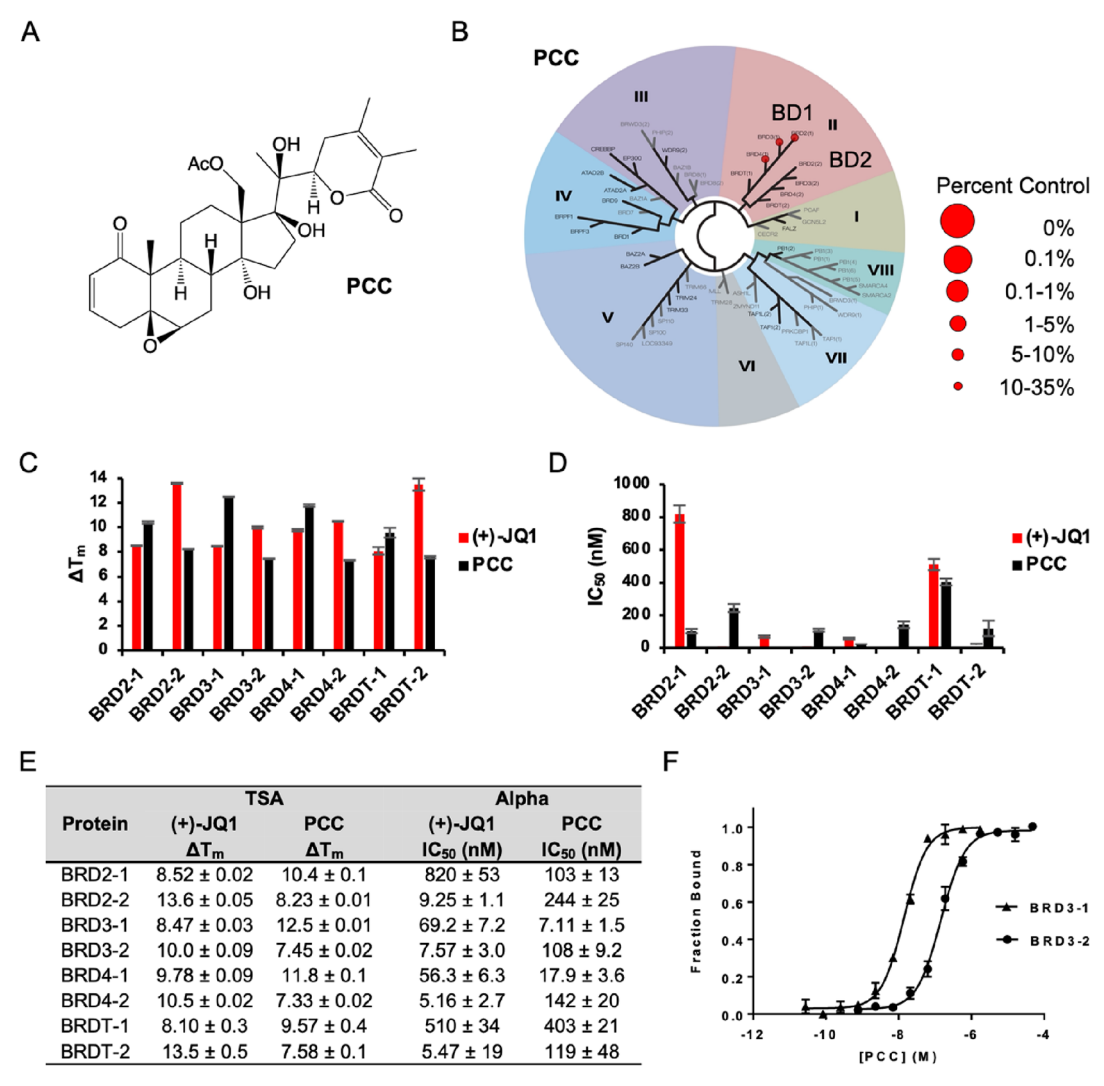


Figure 1. PCC binds and inhibits BRDs with selectivity toward BRD3-BD1 and BRD4-BD1. (A) Structure of PCC. (B) BROMOscan bromodomain profiling of PCC using the BROMOscan bromodomain competition binding assay performed by the Eurofins DiscoverX Corporation. Phylogenetic tree of bromodomains demonstrating preferential compound binding of 50 nM PCC. Hits were selected based upon 65% or greater inhibition compared to control. (C)  $T_{\rm m}$  shifts (°C) of each bromodomain upon treatment with (+)-JQ1 or PCC in a thermal shift assay using DSF. Error reported is standard error of the mean (SEM). n = 3. (D) IC<sub>50</sub> values (nM) of (+)-JQ1 or PCC disrupting peptide binding to each BRD bromodomain in an Alpha assay. Error reported is SEM. n = 3. (E)  $T_{\rm m}$  shifts (°C) and IC<sub>50</sub> values (nM) from C and D, respectively. (F) PCC binds BRD3-BD1 by MST with a  $K_{\rm d}$  of 14.1  $\pm$  1.5 nM. PCC binds BRD3-BD2 by MST with a  $K_{\rm d}$  of 149  $\pm$  17 nM. Error reported is SEM, n = 3.

directly modulate the expression of specific disease-promoting genes.

The BET family of proteins were recently shown to be involved in PC progression to CRPC through transcriptional activation of AR. 19 Although BET inhibitors had been utilized to treat cancers such as NUT midline carcinoma<sup>20</sup> and lymphoma,<sup>21</sup> these findings led to pre-clinical studies investigating the use of BET inhibitors to treat CRPC. Most of these studies used (+)-JQ1 (hereinafter referred to as JQ1),<sup>22</sup> a potent thienotriazolodiazepine-inhibitor of BET proteins that has been shown to repress expression of anti-apoptotic factors in ARpositive PC cell lines while also reducing transcription of AR target genes.<sup>23</sup> JQ1 blocks the interaction between BET proteins and the N-terminal domain of AR, limits AR recruitment to DNA independent of androgen binding to AR, and reduces levels of an AR splice variant that confers resistance to ADT as it becomes over-expressed in CRPC. 19 Despite early success, JQ1 has not been approved for clinical use as it has a very short plasma half-life and dose-limiting toxicities.<sup>24</sup> Furthermore, JQ1

is a pan-BET inhibitor, which may narrow its therapeutic window and cause off-target liabilities that limit its effectiveness. <sup>25,26</sup>

The BET family encompasses bromodomain-containing proteins BRD2, BRD3, BRD4, and BRDT, four similar proteins that each have two bromodomains (BD1 and BD2). BRD2, 3, and 4 are ubiquitously expressed, while BRDT is only present in the testes. The BET proteins have a broad range of functions and share many similarities, but the differences among them indicate a possible need for BET inhibitors that are selective within the family to be used as probes to discern BET functions and as potential therapeutics. To illustrate, BRD2 regulates the differentiation of neurons<sup>27</sup> and adipose tissue,<sup>28</sup> while BRD3 modulates gene transcription related to the development of embryonic stem cells<sup>29\*</sup> and facilitates recruitment of the erythroid transcription factor to regulate the maturation of hematopoietic cells. 30,31 BRD4-specific pathways control transcriptional activation in nuclear compartments, 32,33 and BRDT facilitates pathways that regulate spermatogenesis. 34-36 The

**Journal of Medicinal Chemistry** 

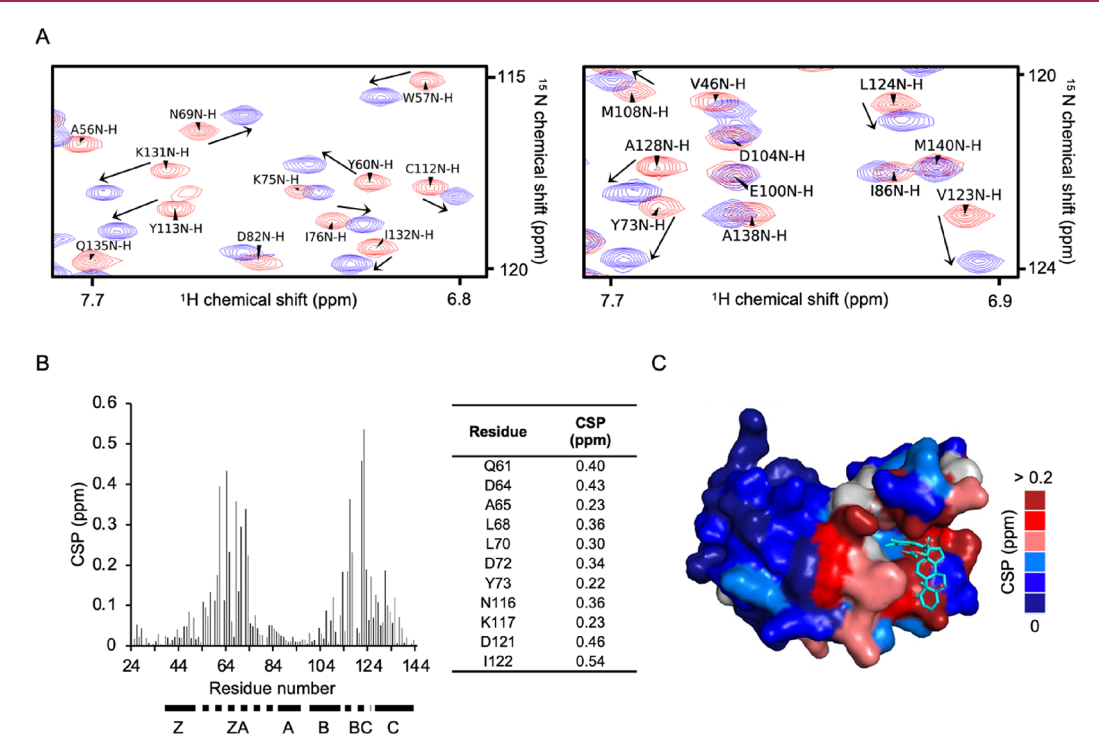


Figure 2. BRD3-BD1 backbone assignments by NMR predict PCC binding site on BRD3-BD1. (A) Portions of <sup>15</sup>N-HSQC spectra of BRD3-BD1 (residues 24-144) in the absence (red, BMRB: 50801) and presence (blue, BMRB: 50802) of one molar equivalent of PCC. Arrows indicate chemical shift perturbations (CSPs) due to the addition of PCC. Apo spectra assignments are labeled in black. (B) CSP distances of each amino acid of <sup>15</sup>N-BRD3-BD1 (residues 24-144) upon addition of PCC. Proline shifts are shown as zero as they produce no signal in <sup>15</sup>N-HSQC experiments. Domain architecture of BRD3-BD1 is indicated under the graph. Solid lines indicate helices. Dashed lines indicate loops. Residues with CSPs greater than two standard deviations from zero (greater than 0.2 ppm) are listed in the table. (C) Surface representation of an X-ray crystal structure of PCC bound to BRD3-BD1 (PDB: 7R8R) colored based on the CSP distance upon addition of PCC. Prolines are colored gray.

presence of BD1 and BD2 within each BRD protein adds another level of complexity to the BET selectivity problem. BD1 primarily serves as a chromatin-binding module, and BD2 is typically used for transcription factor recruitment.<sup>37</sup> Selective BD1 and BD2 inhibitors are also of interest, and preliminary research indicates that BD1 is crucial for steady-state gene expression, while both BD1 and BD2 are required for rapid increase of gene expression induced by inflammatory stimuli.<sup>38</sup> This suggests the possibility that BD1 inhibitors are more effective in cancer, while BD2 inhibitors may be more successful in inflammatory and autoimmune diseases. Given the broad involvement of BETs in transcriptional regulation and the lack of selectivity and poor pharmacokinetics of JQ1, BET inhibitors with improved selectivity and pharmacokinetic profiles are needed to dissect BET biology and reach the clinical potential of

A high-throughput screen of over 18,000 natural product samples for inhibitors of androgen-induced gene expression identified a natural product of the  $17\beta$ -hydroxywithanolide (17-BHW) class, physachenolide C (PCC), as a promising hit that inhibited the expression pattern of a subset of genes involved in PC. 39 Subsequently, a biotinylated analogue of PCC (Bt-PCC) was incubated with cellular extracts, and a pulldown accompanied by mass spectrometry analysis identified the BET family of proteins as potential cellular targets of PCC. 40 Target validation, structural biology, and cytotoxicity assays in PC cells identified PCC as a BET inhibitor with selectivity for BRD3-BD1 and BRD4-BD1. PCC also degrades BRD3 and BRD4 through the ubiquitin proteasome pathway (UPP), possibly acting as a molecular glue. Finally, PCC is more

efficacious than JQ1 against AR-positive PC cells and retains reasonable potency against AR-negative CRPC cells that are resistant to JQ1.

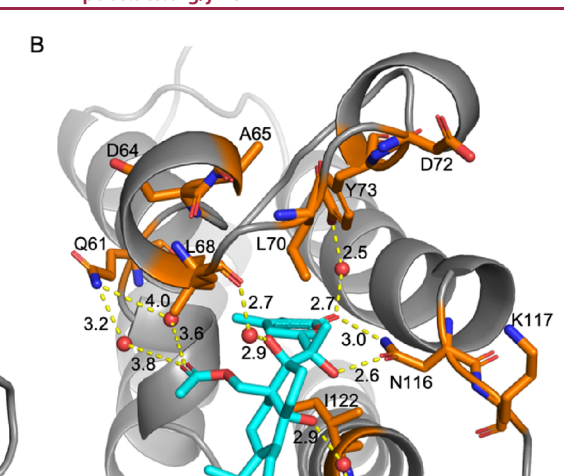
#### **RESULTS**

The selectivity of PCC (Figure 1A) among bromodomaincontaining proteins was initially investigated using BROMOscan bromodomain competition binding assays (Eurofins DiscoverX Corporation). PCC selectively inhibited immobilized-ligand binding to BD1 of BET family bromodomains BRD2, BRD3, and BRD4 (Figure 1B). Both individual BDs of each BET family BRD were recombinantly produced and purified (Figure S1), and primary biochemical studies were performed to validate each BD as a target of PCC and compare PCC to pan-BET inhibitor JQ1. 13 The interactions between each BD and either PCC or JQ1 were initially compared by thermal shift assay (TSA) using differential scanning fluorimetry (DSF). Addition of PCC or JQ1 caused positive melting temperature  $(T_m)$  shifts for both BDs of each BRD, indicating that both PCC and JQ1 bind and stabilize all BET family bromodomains (Figure 1C,E). Furthermore, and in accordance with the BROMOscan results, PCC caused larger  $T_{\rm m}$  shifts for each BD1 than it did for each BD2, suggesting that PCC may bind each BET family BD1 tighter than each BD2.

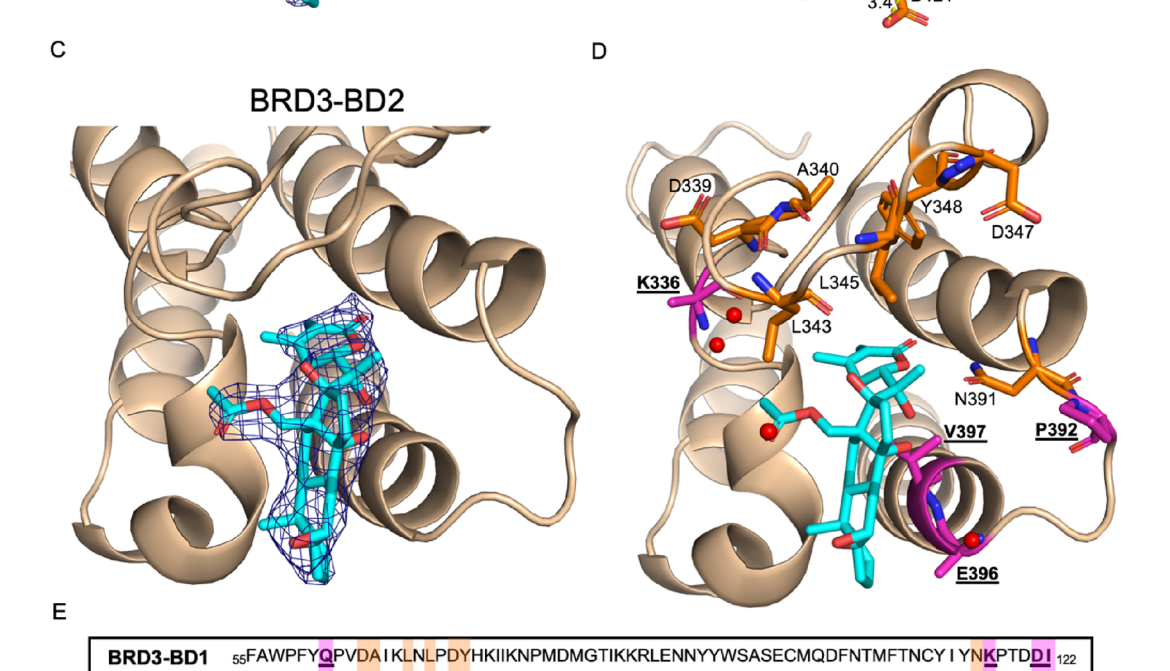
A well-established amplified luminescent proximity homogeneous (Alpha) assay41 was employed to further probe the selectivity trends of PCC and JQ1 and directly measure inhibition of K<sub>ac</sub>-peptide binding to each BET family BD. Dose responses were performed for both BDs of each BRD, and the same trends exhibited by TSA were reinforced (Figure

Journal of Medicinal Chemistry pubs.acs.org/jmc

BRD3-BD1



Article



BC loop

Figure 3. X-ray crystal structures of PCC bound to BRD3-BD1 (PDB: 7R8R) and BRD3-BD2 (PDB: 7S3P). (A)  $2F_o$ - $F_c$  omit map showing electron density (contoured at 1.5 $\sigma$ ) for PCC (cyan) bound to BRD3-BD1. (B) Front view of PCC bound to BRD3-BD1. Amino acids whose <sup>15</sup>N-HSQC CSPs are greater than two standard deviations from zero are labeled and shown as orange sticks. Relevant waters are shown as red spheres. Hydrogen bond interactions between PCC and BRD3-BD1 are shown as yellow dashes. Distances indicated are angstroms. (C)  $2F_o$ - $F_c$  omit map showing electron density (contoured at 1.5 $\sigma$ ) for PCC (cyan) bound to BRD3-BD2. (D) Amino acids with large BRD3-BD1 <sup>15</sup>N-HSQC CSPs were aligned to BRD3-BD2 and are labeled and shown as colored sticks. Within those, amino acids shown in pink, bolded, and underlined are not conserved between BRD3-BD1 and BRD3-BD2. Waters are shown as red spheres. (E) Partial sequence alignment of BRD3-BD1 and BRD3-BD2. Same labeling in (D) applies in (E).

ZA loop

330YAWPFYKPVDAEALELHDYHDIIKHPMDLSTVKRKMDGREYPDAQGFAADVRLMFSNCYKYNPPDHEV 397

1D,E). PCC was a more potent inhibitor of each BD1 than BD2, with the exception of BRDT, which is only expressed in the testes,  $^{34}$  and PCC was a more potent inhibitor of each BD1 than JQ1. Furthermore, PCC was most potent against BRD3-BD1 and BRD4-BD1 in the Alpha assay and displayed greater than five-fold selectivity for these two BDs over all others. Between these two BD1s, PCC was more potent against BRD3-BD1, exhibiting a low nanomolar IC $_{50}$  and greater than 10-fold selectivity for BRD3-BD1 over BRD3-BD2. Next, microscale thermophoresis (MST) was used to investigate the BRD3 BD

BRD3-BD2

selectivity of PCC in direct-binding measurements. Dose responses of PCC were performed with both BDs, and the potency and selectivity were corroborated. PCC binds about 10-fold tighter to BRD3-BD1 than BRD3-BD2, and the  $K_{\rm d}$  of PCC for BRD3-BD1 is in the low nanomolar range (Figure 1F). Taken together, the BROMOscan, TSA, Alpha, and MST data indicate that PCC displays enhanced selectivity and potency toward BRD3-BD1 and BRD4-BD1.

**BC** loop

Uniformly <sup>13</sup>C, <sup>15</sup>N-labeled BRD3-BD1 (residues 24–144) was expressed and purified for NMR experiments to explore

Table 1. Cell Viability Data

				cell line <sup>b</sup>			
compound	VCaP	LNCaP	22Rv1	DU-145	PC-3	HFF	WI-38
PCC	$30.5 \pm 5.0$	$21.6 \pm 0.9$	$30.3 \pm 5.0$	$263.0 \pm 12.0$	$63.0 \pm 12.0$	>2000 <sup>d</sup>	NT <sup>c</sup>
1	$NT^c$	$60.0 \pm 10.0^d$	$70.0 \pm 10.0^d$	$\mathrm{NT}^c$	$NT^c$	>10,000 <sup>g</sup>	$NT^c$
2	$NT^c$	$130.0 \pm 10.0^d$	$70.0 \pm 20.0^d$	$NT^c$	$130.0 \pm 0.01^{e}$	>3000 <sup>e</sup>	$NT^c$
3	$NT^c$	$1100.0 \pm 100.0^{e}$	$NT^c$	$NT^c$	$3100.0 \pm 200.0^{e}$	>3000 <sup>e</sup>	$NT^c$
4	$NT^c$	$412.3 \pm 24.6$	$177.0 \pm 11.7$	$1468.1 \pm 16.9$	$424.8 \pm 17.2$	>2000	$NT^c$
5	$NT^c$	$320.0 \pm 80.0^{e}$	$NT^c$	$NT^c$	$1200.0 \pm 100.0^{e}$	>12,000	$NT^c$
6	$NT^c$	$1200.0 \pm 100.0^{e}$	$NT^c$	$NT^c$	$180.0 \pm 100.0^{f}$	$NT^c$	>5000
7	$NT^c$	$290.0 \pm 50.0^d$	$210.0 \pm 20.0^d$	$NT^c$	$NT^c$	>2000 <sup>d</sup>	$NT^c$
8	$1110.0 \pm 190.0$	$2780.0 \pm 660.0$	$NT^c$	>5000	$2900.0 \pm 320.0$	$NT^c$	>5000
9	$NT^c$	$870.0 \pm 10.0^{e}$	$NT^c$	$NT^c$	$410.0 \pm 10.0^{b}$	>6800 <sup>e</sup>	$NT^c$
10	$NT^c$	>2000	>2000	>2000	>2000	>2000	$\mathrm{NT}^c$
11	$NT^c$	$1060.9 \pm 104.8$	$1494.2 \pm 302.0$	>2000	$844.0 \pm 197.0$	>2000	$NT^c$
12	$NT^c$	$1052.3 \pm 192.7$	$1131.6 \pm 488.8$	>2000	$899.0 \pm 7.7$	>2000	$NT^c$
13	>2000	$NT^c$	$NT^c$	$NT^c$	$1098.0 \pm 198.0$	$NT^c$	$NT^c$
(+)-JQ1	$160.3 \pm 9.5$	$162.0 \pm 12.7$	$230.5 \pm 4.9$	>2000	>2000	>2000	$NT^c$
doxorubicin	$670.0 \pm 60.0$	$110.0 \pm 20.0$	$20.0 \pm 1.0$	$40.0 \pm 10.0$	$340.0 \pm 50.0$	$150.0 \pm 30.0$	$800.0 \pm 80.$

"Results are expressed as EC<sub>50</sub> values in nM. Doxorubicin and DMSO were used as positive and negative controls, respectively. "Key: PC-3 = human prostate adenocarcinoma; LNCaP = human hormone-responsive PSA-expressing prostate adenocarcinoma; DU-145 = human androgen receptor-positive and PSA non-expressing prostate adenocarcinoma; VCaP = metastatic human prostate adenocarcinoma; 22Rv1 = human prostate PSA-expressing and androgen receptor-positive carcinoma epithelial cells; HFF = human foreskin fibroblast cells. "NT = Not tested. "Ref 43. "Ref 39. "Ref 46. "Ref 44."

which BRD3-BD1 amino acids are affected by PCC binding. The  $^{15}$ N-heteronuclear single quantum coherence (HSQC) spectra of both the apo (BMRB: 50801) and the PCC-bound (BMRB: 50802) BRD3-BD1 displayed excellent peak dispersion, and the backbone of the protein was assigned in each condition (Figure 2A). Backbones of both apo and bound spectra were assigned to ensure correct identification of chemical shift perturbations (CSPs). Many CSPs were observed upon overlaying the  $^{15}$ N-HSQC spectra of the apo and bound proteins, indicating tight, uniform binding of PCC to BRD3-BD1. Each peak displayed a different shift profile, and the distance of each CSP was calculated using the following equation where  $\delta$ H and  $\delta$ N refer to the chemical shifts on the  $^{14}$ H and  $^{15}$ N axes of the  $^{15}$ N-HSQC, respectively.

$$CSP = \frac{\sqrt{(\delta H_{PCC} - \delta H_{apo})^2 + [0.2 \times (\delta N_{PCC} - \delta N_{apo})]^2}}$$

 $\Delta \delta N$  is multiplied by 0.2 to remove bias toward shifts in the N dimension because the spectral range of chemical shifts for N is much larger than for H. Residues that produced the largest CSPs exist in two distinct regions of BRD3-BD1: from Q61 to Y73 and from N116 to I122 (Figure 2B). These two regions are known as the ZA and BC loops, respectively, which connect the four alpha helices (Z, A, B, and C) that comprise the BD structure and surround the central K<sub>ac</sub> binding pocket of BRD3-BD1. CSP magnitudes were assigned to a color gradient, and the colors were applied to a surface representation of an X-ray crystal structure of BRD3-BD1 (PDB: 7R8R). One half of the protein is characterized by small CSPs (blues), while the other half, comprising the ZA and BC loops, has many large CSPs (red) (Figure 2C). Large CSP shifts indicate that either PCC makes direct interactions with these residues or binding of PCC to BRD3-BD1 causes structural changes in the protein that directly affect the positioning and molecular environment of these amino acids. The area encompassed by the ZA and BC loops, characterized by amino acids with large CSPs, was hypothesized as the PCC binding pocket.

A 1.8 Å resolution X-ray crystal structure of PCC in complex with BRD3-BD1 (Table S1, PDB: 7R8R) confirmed the location of the PCC binding pocket and revealed the binding pose of PCC (Figure 3A). PCC engages the K<sub>ac</sub> binding pocket encompassed by the ZA and BC loops of BRD3-BD1 and is in position to block binding of  $K_{ac}$  substrates. The  $\delta$ -lactone moiety of PCC reaches into the binding pocket and the lactone methyl groups are forced back, away from solvent. In addition, there is no density to suggest that PCC covalently inhibits BRD3-BD1 through its unsaturated  $\delta$ -lactone moiety. This binding pose is corroborated by the Bt-PCC pulldown experiment, in which Bt-PCC is biotinylated on its solvent-accessible A ring. 40 As predicted, amino acids that exhibited CSPs greater than two standard deviations from zero (greater than 0.2 ppm) by NMR surround the binding pocket of PCC (Figure 3B and Figure S2A), and although many residues encompass the pocket, only the residues with the largest CSPs are positioned to form binding interactions with the inhibitor. In the X-ray crystal structure, PCC directly engages N116 of BRD3-BD1 with two hydrogen bonds. In BRD3-BD1, N116 is the conserved asparagine, a residue which is crucial for the anchoring of Kac substrates to BRDs. Engagement of this conserved asparagine is likely the interaction that most strongly drives BRD inhibition. 13 Furthermore, PCC engages the backbone carbonyl of L68 and the side chains of Q61, Y73, and D121 of BRD3-BD1 through water bridges. Specifically, there are four water molecules that are oriented between Q61 and the acetyl carbonyl of PCC (Figure S2B), which the acetyl moiety may engage to fortify its binding interaction with BRD3-BD1.

An X-ray crystal structure of BRD3-BD2 bound to PCC (Table S1, PDB: 7S3P) was solved to understand the greater than 10-fold selectivity of PCC for BRD3-BD1 over BRD3-BD2 (Figure 3C). PCC assumes the same pose in both pockets and is poised to make many similar binding interactions between both bromodomains (Figure 3D). However, although BRD3-BD1

**Journal of Medicinal Chemistry** 

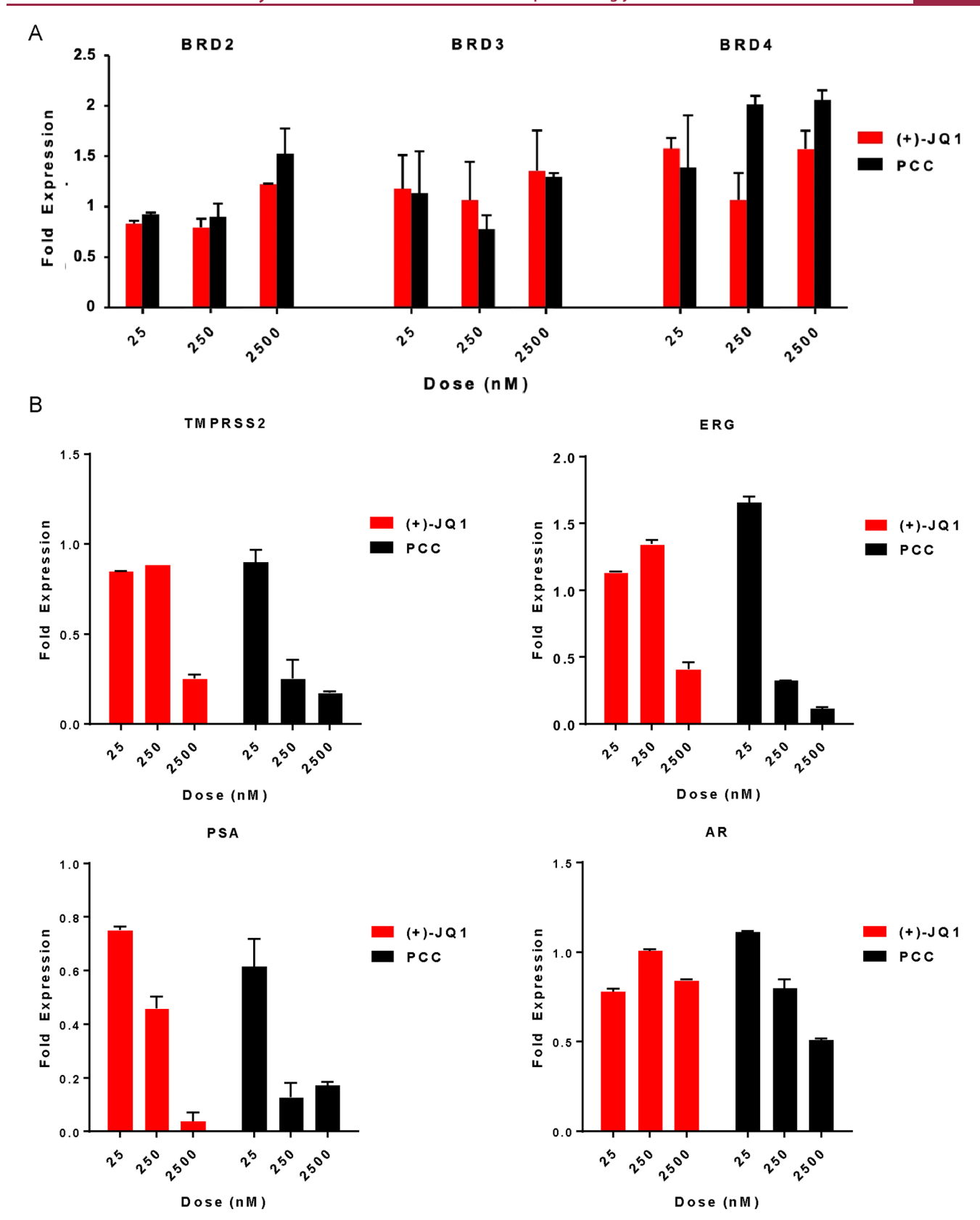


Figure 4. Effects of PCC treatment on BET, AR, and AR target gene mRNA in VCaP cells. (A, B) Quantitative reverse transcription polymerase chain reaction (qRT-PCR) analysis of indicated genes in VCaP cells treated with PCC or (+)-JQ1 for 24 h. Data shown are the mean of three independent experiments. Error reported is SEM (n = 3).

and BRD3-BD2 share many structural features, there are

to PCC selectivity. Q61, K117, D121, and I122 in BRD3-BD1

differences between their ZA and BC loops that may contribute (K336, P392, E396, and V397, respectively, in BRD3-BD2) all

#### Scheme 1. Preparation of PCC-NHS-Fluorescein Conjugate 14<sup>a</sup>

"Reagents and conditions: (a) SeO<sub>2</sub>, anhy. CH<sub>2</sub>Cl<sub>2</sub>, under N<sub>2</sub>, 25 °C, 24 h, reflux, 30 h. (b) *m*-CPBA, CH<sub>2</sub>Cl<sub>2</sub>, 25 °C, 3 h. (c) Fmoc-glycine, DCC, 4-pp, anhy. EtOAc, 25 °C, 1.5 h. (d) TBAF, THF, 0 °C, 1 h. (e) anhy. DMF, 25 °C, 4 h.

displayed large CSPs by NMR upon addition of PCC, and these residues are not conserved between BRD3-BD1 and BRD3-BD2 (Figure 3E). Furthermore, Q61 and D121 form hydrogen bond interactions through water with PCC in the BRD3-BD1 X-ray crystal structure. This water-bridging hydrogen bond interaction with D121 has been targeted by others to confer BD1 selectivity.<sup>38</sup> In the BRD3-BD2 crystal structure, the acetoxy carbonyl of PCC is predicted to rotate away from K336 (Q61 in BRD3-BD1), and there is no available water network for PCC to engage E396 (D121 in BRD3-BD1) through hydrogen bonds. In addition, K336 and E396 both showed disperse electron densities for their side chains, indicating that they are flexible and not engaged by PCC. The inability of PCC to access binding interactions with non-conserved residues K336 and E396 in BRD3-BD2 likely explain the greater than 10-fold selectivity of PCC for BRD3-BD1 over BRD3-BD2.

Although PCC and JQ1 occupy the same binding pocket, PCC engages Q61 and D121 (Figure 3B) while JQ1 does not (Figure S2C). In PCC-bound BRD3-BD1, the Q61 side chain swings in toward the binding pocket, allowing an interaction with PCC (Figures S2A and S2B), and in JQ1-bound BRD3-BD1, the Q61 side chain points away from JQ1 and into solvent (Figure S2C). The differences between the PCC and JQ1 binding pocket interactions and, specifically, the ability of PCC

to make hydrogen bonds with Q61 and D121 may explain why PCC is more potent and selective for BRD3-BD1 than JQ1 (Figure 1D,E).

Cellular potencies of PCC and JQ1 were compared in a cell viability assay using androgen receptor (AR)-positive VCaP human PC cells that are preferentially sensitive to JQ1. 19 PCC and JQ1 both decreased VCaP cell viability with EC50 values in the nanomolar range while leaving non-cancerous HFF cells relatively unaffected (Table 1). However, PCC was about 5-fold more potent than JQ1. qRT-PCR experiments were performed using the VCaP cells to compare the effects of PCC and JQ1 on BRD mRNA and AR target genes. Neither PCC nor JQ1 treatment decreased mRNA levels of BRD2, BRD3, or BRD4 in VCaP cells (Figure 4A). VCaP cells, which have the TMPRSS2-ERG gene fusion and AR amplification, showed a dosedependent decrease in TMPRSS2, ERG, and prostate-specific antigen (PSA) at the messenger RNA level upon PCC or JQ1 treatment (Figure 4B). However, about 10-fold less PCC was required to elicit these mRNA effects. Additionally, while treatment with JQ1 left AR mRNA relatively unchanged, AR mRNA showed a dose-dependent decrease in VCaP cells after treatment with PCC.

A new high-throughput fluorescence polarization (FP) assay was developed to facilitate biochemical testing of additional

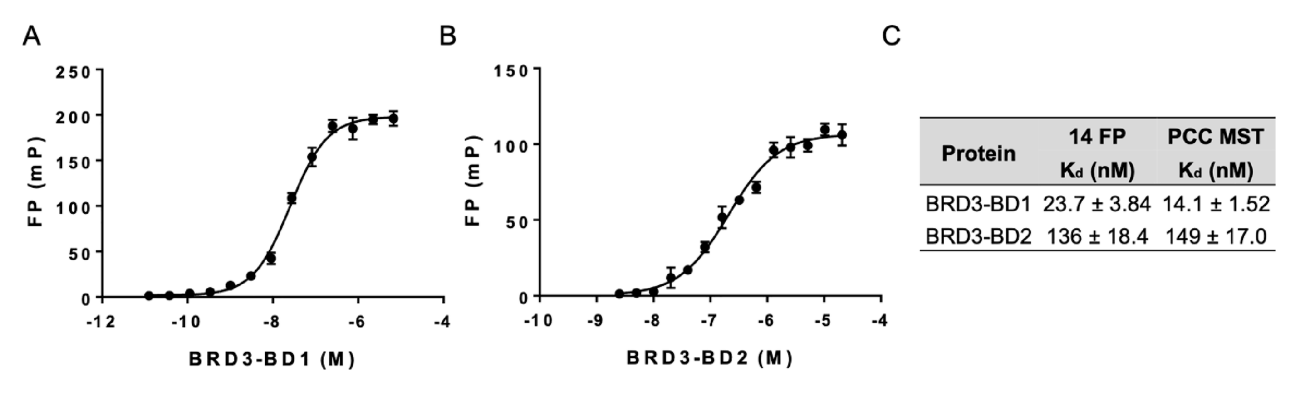


**Figure 5.** Fluorescent probe **14** binds BRD3 bromodomains. (A)  $K_d$  of **14** binding to BRD3-BD1 and (B) BRD3-BD2 by FP. (C) Potency and selectivity of **14** for BRD3-BD1 and BRD3-BD2 by FP match those of PCC from MST experiments.

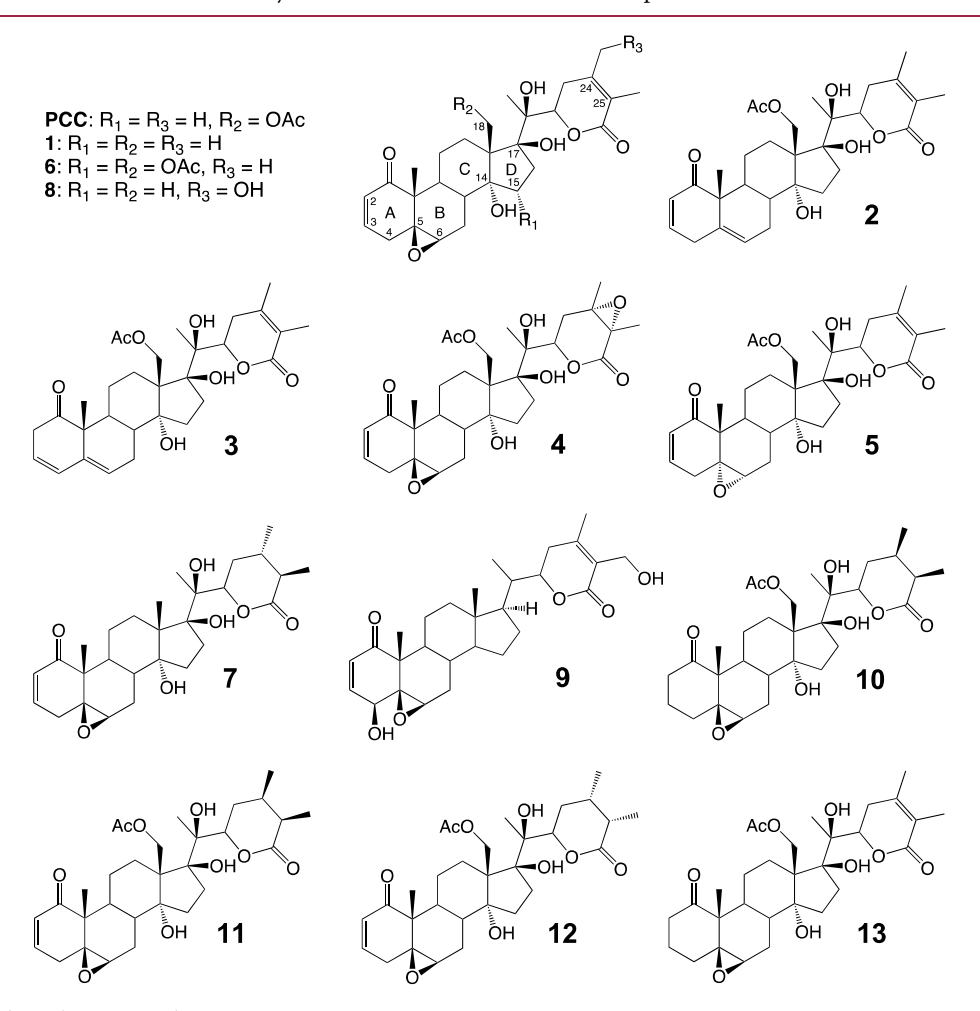


Figure 6. Withanolide analogues tested.

with anolide analogues as Alpha and MST can be cost-prohibitive and time-consuming. Potency in the FP assay is determined by the ability of each inhibitor to compete a BRDbinding fluorophore out of its binding pocket. The BRD-binding  $K_{ac}$  peptide from the Alpha assay with a FAM fluorophore attached was initially produced to act as the fluorophore in this FP assay. However, the FAM-peptide showed a very weak interaction with the BRD protein, presumably because the fluorophore disrupted the binding. Therefore, high affinity interactions could not be measured using this peptide. To circumvent this, a fluorescent PCC analogue (14) was produced to serve as the fluorophore in this FP assay (Scheme 1). Fluorescent analogue 14 was synthesized beginning with hydroxylation of 2 at the 4-position to produce intermediate 20. Epoxidation of 20 yielded intermediate 21, whose 4-hydroxyl was subsequently alkylated with Fmoc-glycine to produce intermediate 22. Deprotection of 22 yielded free amine 23, which was conjugated to NHS-Fluorescein to produce PCC-NHS-Fluorescein conjugate 14. This molecule was designed with the fluorescein moiety extending off the A-ring as this region is solvent-exposed in the X-ray crystal structures of BRD3-BD1 and BRD3-BD2 bound to PCC (Figure 3). Binding of compound 14 was initially tested by FP against BRD3-BD1 and BRD3-BD2 (Figure 5A,B). The potency of 14 for each BD

agreed with the  $K_d$  values by MST for PCC as 14 was also 5- to 10-fold more potent for BRD3-BD1 over BRD3-BD2 (Figure 5C).

A small library of withanolide analogues with varying functionalities was used to probe potential interactions in the BRD binding pocket (Figure 6). Naturally occurring withanolides used in this study were obtained from aerial parts of aeroponically cultivated *Physalis peruviana* (1, 7), <sup>43,44</sup> *Physalis crassifolia* (PCC, 2, 3, and 6), <sup>45,46</sup> *Physalis coztomatl* (8), and *Withania somnifeara* (9). <sup>47</sup> Analogues 4, 5, and 13 were obtained as described previously. <sup>45</sup> Three additional withanolide analogues were also synthesized and utilized in this study. Reduction of the 2,3 and 24,25 double bonds of PCC produced 10 (Scheme 2). 24,25-Racemates 11 and 12 were produced

## Scheme 2. Preparation of (24*R*,25*R*)-2,3,24,25-Tetrahydrophysachenolide C (10)<sup>a</sup>

<sup>a</sup>Reagents and conditions: (a) Pt/C, under H<sub>2</sub>, EtOH, 36 h.

starting with reduction and hydroxylation of 2 at the 3-position to yield intermediate 15. Silylation of 15 provided protected intermediate 16, which was subsequently epoxidated to produce intermediate 17. Reduction of the 24,25-double bond yielded racemic mixture 18, which was deprotected to produce intermediate mixture 19. The 2,3-double bond was then regenerated, and the enantiomers were separated to provide withanolide analogues 11 and 12 (Scheme 3).

Withanolide analogues were tested for biochemical potency in the FP assay. In general, analogues showed strong selectivity toward BD1 over BD2 (Table 2 and Table S2). Compounds 2,

Table 2. BRD3 and BRD4 FP Assay Data<sup>a</sup>

compound	BRD3-BD1	BRD3-BD2	BRD4-BD1	BRD4-BD2
1	$2949 \pm 943$	$720.3 \pm 91.9$	$556.2 \pm 80.6$	$1523 \pm 829$
2	$18 \pm 1.7$	$15,820 \pm 1662$	$19.3 \pm 8.3$	$3917 \pm 463$
3	$262 \pm 109$	$130.7 \pm 67.9$	$909 \pm 76.1$	$294 \pm 106$
4	$2356 \pm 1215$	$754.7 \pm 165$	$1934 \pm 76.7$	$5626 \pm 1360$
5	$89.7 \pm 4.7$	$4256 \pm 1580$	$31.2 \pm 4.7$	$10,770 \pm 3730$
6	$210\pm21$	$6002 \pm 2540$	$47.6 \pm 5.6$	$14,770 \pm 1520$
8	$736 \pm 53.9$	>20,000	$281 \pm 51.9$	>20,000
9	>20,000	>20,000	>20,000	>20,000
10	>20,000	>20,000	$3875 \pm 1031$	$1834 \pm 938$
11	>20,000	>20,000	>20,000	>20,000
12	>20,000	>20,000	>20,000	>20,000
13	$235 \pm 11.5$	$10,550 \pm 1140$	$60 \pm 6.1$	$9144 \pm 2140$

<sup>a</sup>Results are expressed as IC<sub>50</sub> values in nM  $\pm$  SEM. n = 3.

5, 6, and 13 were at least 30-fold selective for BRD3-BD1 and BRD4-BD1 over BRD3-BD2 and BRD4-BD2, compared to compound 1, which had no selectivity between BRD3 and BRD4 bromodomains. Furthermore, 2, 5, 6, and 13 have acetoxy groups at their C-18 positions while 1 does not (Figure 6), again demonstrating that engagement of Q61 is likely a main driver of withanolide selectivity for BRD3-BD1 over BRD3-BD2. In addition, analogues 4, 10, 11, and 12 are not potent for BRD3-BD1 or BRD4-BD1, and each of these compounds feature saturation of the  $\delta$ -lactone double bond. This implies that an unsaturated lactone is important for inhibition of BRD3-BD1 and BRD4-BD1. For BRD3-BD1, this is likely because the saturated lactone assumes different stereochemical orientations, possibly interrupting hydrogen bond interactions to Y73 and

Scheme 3. Preparation of 24,25-Dihydro-PCC Analogues (11 and 12)<sup>a</sup>

"Reagents and conditions: (a) 1. B<sub>2</sub>(pin)<sub>2</sub>, CuCl<sub>2</sub>, Et<sub>3</sub>N, THF, H<sub>2</sub>O, 25 °C, 15 min. 2. NaBO<sub>3</sub>. 4H<sub>2</sub>O, 25 °C, 15 min. (b) *t*-BDMSiCl, 4-pp, DMF, 60 °C, 16 h. (c) *m*-CPBA, CH<sub>2</sub>Cl<sub>2</sub>, 25 °C, 3 h. (d) Pd/C, under H<sub>2</sub>, EtOH, 24 h. (e) TBAF, THF, 0 °C, 30 min. (f) 1. *p*-Nitrobenzoic acid, DCC, 4-pp, EtOAc, 25 °C, 4 h. 2. Excess 4-pp, 16 h. 3. Repeated prep TLC.

ī

Journal of Medicinal Chemistry pubs.acs.org/jmc

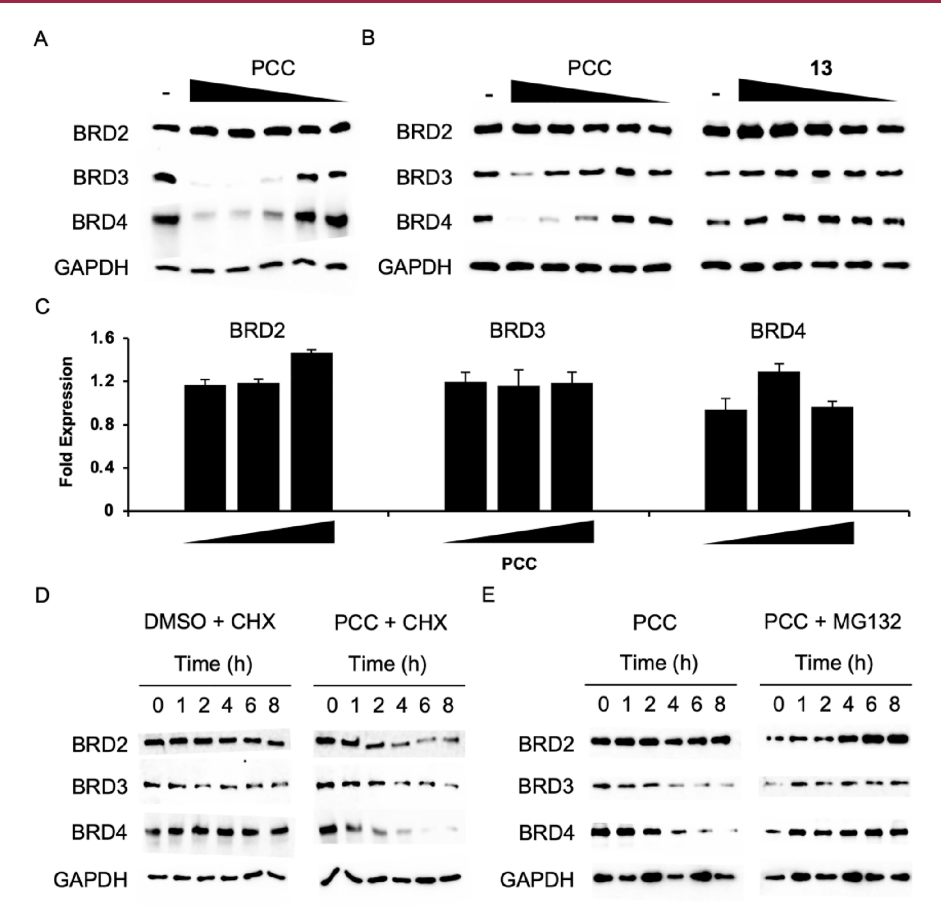


Figure 7. Effects of inhibitor treatment or cotreatment on protein and mRNA levels of BRD2, BRD3, and BRD4. (A) MDA-MB-231 cells were treated with PCC for 16 h. PCC doses decrease 10-fold from 10  $\mu$ M to 1 nM. PCC BRD2 DC<sub>50</sub> > 10  $\mu$ M, PCC BRD3 DC<sub>50</sub> = 23.9  $\pm$  21.9 nM. PCC BRD4 DC<sub>50</sub> = 41.6  $\pm$  29.7 nM. Error reported is SEM (n = 2). (B) PC-3 cells were treated with PCC or 13 for 16 h. Doses decrease 10-fold from 10  $\mu$ M to 1 nM. PCC BRD2 DC<sub>50</sub> > 10  $\mu$ M, PCC BRD3 DC<sub>50</sub> = 7290  $\pm$  2830 nM. PCC BRD4 DC<sub>50</sub> = 56.7  $\pm$  34.7 nM. Error reported is SEM (n = 2). (C) Quantitative reverse transcription polymerase chain reaction (qRT-PCR) analysis of indicated genes in MDA-MB-231 cells treated with PCC for 24 h. PCC doses increase tenfold from 25 nM to 2.5  $\mu$ M. Error reported is SEM (n = 3). (D) MDA-MB-231 immunoblots of cells treated during a time-course with 50 ug/mL  $\mu$ M CHX and DMSO or 50  $\mu$ g/mL CHX and 10 uM PCC. (E) MDA-MB-231 immunoblots of cells treated during a time-course with 10  $\mu$ M PCC and DMSO or 10  $\mu$ M PCC and 10  $\mu$ M MG132.

N116 and perturbing the positions of its methyl groups. Finally, compound **2**, which has an unsaturated B ring and no epoxide, is over 10-fold more potent for BRD3-BD1 and BRD4-BD1 than **3**, which has no epoxide and a conjugated A-B ring system. Altering the stereochemistry of the epoxide on the B-ring in compound **5** also results in a drop in BRD3-BD1 and BRD4-BD1 potency relative to **2**, although **5** is still quite potent and selective for these two bromodomains.

Cell viability studies in LNCaP prostate adenocarcinoma cells were initiated to elucidate how biochemical SAR between with anolide analogues and BETs correlates to cellular potency of withanolides. LNCaP cells are AR-positive, express PSA, and are highly sensitive to BET inhibition. 19 PCC potently decreased LNCaP cell viability, with an EC<sub>50</sub> of about 20 nM, which was over 7-fold more potent than JQ1 (Table 1). In general, other withanolide analogues did not show improved cellular potency. Withaferin A (9) is unique from the other withanolide analogues, in part due to its  $\beta$ -oriented C-17 side chain (Figure 6). Withaferin A also lacks hydroxyl groups at C-14 and C-17, preventing formation of hydrogen bond interactions with BRD3-BD1 D121 and the backbone carbonyl of L68. Compound 6 features an acetoxy group at C-18 and exhibits a micromolar  $EC_{50}$  in LNCaP cells as this acetoxy is not positioned to form interactions with the binding pocket.

Compounds 1, 7, 8, and 9 lack the acetoxy group at C-18, which eliminates the possibility for hydrogen bond interactions with Q61. Analogues 1, 8, and 9 experience losses in potency for BRD3-BD1 and BRD4-BD1 in FP experiments (7 was not tested), and all four compounds lose potency in the LNCaP cell viability assay, reinforcing the importance of this acetoxy group to the cellular potency of PCC. Addition of a hydroxyl group to a lactone methyl (8 or 9) also greatly decreased cellular potency. Furthermore, and in accordance with fluorescence polarization data, 4, 7, 10, 11, and 12 feature saturation of the  $\delta$ -lactone double bond, possibly perturbing hydrogen bond interactions to Y73 and N116. Results from compounds 4 and 7-12 suggest that modifications to the lactone of PCC are not well tolerated in cells as it may be difficult to improve upon the hydrophobic interactions between PCC and the back of the binding pocket while preserving hydrogen bonds to Y73 and N116. Compounds 2, 3, and 5 also exhibit consistent potency trends between BRD3-BD1 and BRD4-BD1 FP and LNCaP cell viability studies. Replacement of the epoxide on the B ring with a double bond (2) results in a loss of potency in LNCaP cells, but 2 is almost 10-fold more potent than 3, which has a similar modification with a conjugated ring system. Changing the stereochemistry of the epoxide on the A-ring (5) results in a tenfold drop in potency relative to PCC, although 5 still inhibits

Article

in the nanomolar range. Furthermore, compounds 3, 10, and 13 have saturated A rings, which likely contribute to their loss of potency in LNCaP cells and VCaP cells. Taken together, observations from compounds 2, 3, 5, 10, and 13 suggest that the stereochemical orientation of the epoxide and the presence of an unsaturated A ring are critical for cellular potency. This is possibly because these moieties determine the conformation of the withanolide ring system, which positions the molecular substituents of PCC to make critical interactions with the binding pocket.

PCC, JQ1, and other select with anolide analogues were tested in cell viability assays across different PC cell lines to explore their different cellular potency profiles (Table 1). PCC was over 7-fold more potent than JQ1 in AR-positive, PSA-expressing, 22Rv1 prostate carcinoma epithelial cells. Surprisingly, general potency trends for PCC and its derivatives were consistent in AR-negative, PSA non-expressing DU-145 prostate adenocarcinoma cells, where PCC had an EC<sub>50</sub> in the high nanomolar range. JQ1 was ineffective at concentrations up to 2  $\mu$ M in DU-145 cells, in agreement with previous literature. <sup>19</sup> The contrast in effectiveness between PCC and JQ-1 in AR-negative DU-145 cells prompted additional investigation of PCC and JQ1 in AR-negative PC-3 human prostate adenocarcinoma cells. Indeed, PCC exhibited a nanomolar EC<sub>50</sub>, while JQ1 was ineffective up to 2  $\mu$ M.

Cytotoxicity of PCC toward AR-negative PC cells was unexpected. However, previously investigated BET degraders dBET-1 and dBET-2 show potency trends similar to PCC in PC cells. 48 dBET-1 and dBET-2 display single-digit nanomolar EC<sub>50</sub> values in AR-positive LNCaP cells and decrease expression of c-MYC, as is standard for BET inhibitors.<sup>17</sup> These degraders remain potent in AR-negative PC-3 cells (dBET-1 EC<sub>50</sub> = 50 nMin PC-3 cells, dBET-2 EC<sub>50</sub> = 20 nM in PC-3 cells; Figure 1A in Ref 48 despite not decreasing expression of c-MYC (discussed later). Inspired by this observation, MDA-MB-231 cells and PC-3 cells were treated with PCC to investigate BET degradation by PCC. Surprisingly, PCC treatment caused degradation of BRD3 and BRD4 in a dose-dependent manner (Figure 7A,B). It was hypothesized that PCC may act as a molecular glue that can engage a protein that can target BRD3 and BRD4 for degradation. This glue interaction could take place through the PCC A ring enone as it is situated facing into solvent. To test this, PC-3 cells were treated with compound 13, an analogue of PCC that lacks the A ring enone. Compound 13 did not degrade BRD3 or BRD4 in PC-3 cells (Figure 7B), meaning that PCC may be acting as a molecular glue to promote the degradation of BRD3 and BRD4 through its A ring enone.

Quantitative reverse transcription polymerase chain reaction (qRT-PCR) was performed with BET proteins to probe the mechanism of BET degradation upon PCC treatment. BRD3 and BRD4 depletion was not the result of decreased gene transcription as PCC treatment did not decrease BET mRNA levels (Figure 7C). Next, cells were treated with either translation inhibitor cycloheximide (CHX) or co-treated with CHX and PCC to further assess the mode of BET degradation upon PCC treatment. The combination of PCC and CHX decreased the BET half-life more rapidly than CHX treatment alone, indicating that existing BET proteins were degraded upon PCC treatment (Figure 7D). Finally, cells were treated with PCC alone or in combination with MG132, a proteasome inhibitor, to probe the involvement of the proteasome in BET degradation by PCC. PCC alone degraded BRD3 and BRD4 in a time-dependent manner (Figure 7E). However, this degradation

was prevented when PCC was co-treated with MG132, meaning that engagement of BRD3-BD1 and BRD4-BD1 by PCC in cells likely leads to degradation of BRD3 and BRD4 through the ubiquitin—proteasome pathway (UPP).

The UPP consists of E3 ligases that link the polypeptide cofactor, ubiquitin, onto proteins to designate them for degradation by the 26S proteasome. It is possible that PCC acts as a molecular glue by binding BRD3-BD1 and BRD4-BD1, engaging an E3 ligase through its A-ring enone, and targeting BRD3 and BRD4 for ubiquitylation and degradation through the UPP. Bt-PCC, 40 which contains the A ring enone, was utilized in a pulldown experiment accompanied by LC-MS/MS analysis to explore PCC interactors in PC-3 cell lysate and identify E3 ligases that may be responsible for the degradation of BRD3 and BRD4. As expected, this pulldown identified BRD3 and BRD4 as PCC interactors (Figure S3A). This pulldown also identified E3 ligases TRIM25, UBR4, UBR5, ZNF598, and HUWE1 as potential PCC interactors (Figure S3B). Altogether, PCC may act as a molecular glue, linking an E3 ligase to BRD3 and BRD4 through its solvent exposed A ring enone, targeting BRD3 and BRD4 for degradation through the UPP.

With anolide analogues were investigated in AR-negative PC-3 cell viability studies to probe the relationship between the A ring enone and growth inhibition in AR-negative PC cells. Potency trends for with anolide analogues were very similar between AR-positive LNCaP cells and AR-negative PC-3 cells. All with anolide analogues contain an A ring enone except for 3, 10, and 13 (Figure 6). As expected, 3, 10, and 13 were among the least potent analogues tested in PC-3 cells, all exhibiting EC $_{50}$  values over 1  $\mu$ M (Table 1). Specifically, analogue 13 is over 30-fold less potent than PCC in AR-positive VCaP cells and AR-negative PC-3 cells, indicating that PCC likely retains potency in PC cells by acting as a molecular glue through contribution from its A ring enone.

#### DISCUSSION

Withanolides, steroidal lactones found in some plants that have been used as traditional medicines, possess diverse biological activities and have drawn attention for their potential in pharmaceutical research and development.<sup>49</sup> Withanolides have been reported to display in vitro cytotoxic activity against prostate,<sup>39,43</sup> kidney,<sup>45</sup> and breast cancers,<sup>50</sup> but until recently, BET family proteins have not been confirmed as targets of withanolides.

Multiple pan-BET inhibitors are in clinical trials for treating various cancers.<sup>51</sup> Although some are still ongoing, the trials have revealed some clinical problems with pan-BET inhibition, including patients experiencing dose-limiting toxicity and a variety of side effects such as immunodeficiency.<sup>52</sup> Though some trials have been discontinued because of these adverse effects (NCT02369029 and NCT02711137), clinical ineffectiveness may not be due to a problem with bromodomains as pharmaceutical targets. Pan-BET inhibition likely falls victim to a failure to identify patients most likely to benefit from pan-BET treatment, ineffective dosing, or a lack of selectivity within the BET family.<sup>53</sup> The broad range of bromodomain involvement in regulating gene expression makes it difficult to determine which bromodomain is responsible for positive and negative effects of each pan-BET inhibitor. The poor and short-term clinical responses of pan-BET inhibition have expedited the development of inhibitors that are selective within the BET family.

BRD4 has emerged as the most popular target in the BET family, possibly due to its known associations with cancer-

relevant transcriptional regulators including p53, <sup>54</sup> AP-1, <sup>55</sup> NF-κB, <sup>56</sup> and MYC. <sup>57,58</sup> However, two recently developed BRD4-selective inhibitors are being investigated to treat airway inflammation and not cancer, possibly due to a dominant effect on BRD4-BD2. <sup>59</sup> Given the functional redundancies between BRD4 and the other BET proteins, it is difficult to predict which BET protein to target when treating different diseases. Nevertheless, the direction of research toward selectivity is encouraging.

PC is a heterogeneous disease, but its effects are usually conferred through positive regulation of AR signaling. PCC is about 10-fold more potent than JQ1 in PC cells whose phenotype is driven by AR and express PSA (VCaP, LNCaP, and 22Rv1). Additionally, PCC retains reasonable potency in DU-145 and PC-3 cells, which are AR-negative and do not express PSA, while JQ1 is ineffective. PCC is also able to degrade BRD3 and BRD4, and withanolide analogues such as 13 that are unable to degrade BETs lose potency in PC cells. This degradation is possibly due to an interaction between PCC and BD1 of BRD3 and BRD4 as PCC was most potent for these two bromodomains in the Alpha assay (Figure 1D). However, BD1 engagement by PCC has not been validated in cells. Conversely, JQ1 treatment increases cellular levels of BET proteins. 60 The differing responses of the AR-negative PC cells to JQ1 and PCC suggests different consequences of inhibition between the molecules, but it is unclear if these consequences are attributed to the inhibition or degradation of BRD3 or BRD4 or to an off-target effect.

On the one hand, siRNA studies have shown PC cells to be sensitive to genetic silencing of both BRD3 and BRD4.<sup>61</sup> Both proteins are transcriptional co-regulators that affect transcriptional plasticity through chromatin remodeling, and both interact with multiple cell-specific transcription factors. Activity of BRD3 enables CRPC cell growth through its promotion of AR activity<sup>19</sup> and mediates resistance to antiandrogens.<sup>23</sup> BRD4 promotes CRPC cell growth through an interaction with ERG and AR<sup>62</sup> and mediates resistance to ADT.<sup>63</sup> BRD4 depletion by short hairpin RNA inhibits proliferation of AR-negative DU-145 PC cells.<sup>64</sup> Depletion of BRD4 protein levels through knockdown of deubiquitinase (DUB)3 sensitizes DU-145 cells to JQ1 treatment and allows JQ1 to inhibit DU-145 xenograft tumor growth. 65 In addition, BET degraders prevent the upregulation of BET proteins, which is a possible mechanism of PC resistance to BET inhibitors like JQ1.60

Conversely, the activity of PCC toward AR-negative PC cell lines DU-145 and PC-3 may be unrelated to the degradation of BRD3 and BRD4. Although BET degraders dBET-1 and dBET-2 are hyper-potent against AR-positive PC cell lines and remain potent against AR-negative PC cells, they do not decrease c-MYC expression in AR-negative PC cells. However, treatment with BET inhibitors typically leads to suppression of c-MYC transcription. It is unknown whether dBET degraders and PCC induce off-target effects that contribute to potency against AR-negative PC or if degradation of BETs may confer a cytotoxic effect independent of c-MYC. The interactors identified in the Bt-PCC pulldown will be investigated as alternate PCC targets in AR-negative PC cells in future studies.

Molecular glues are small-molecule degraders that induce protein—protein interactions between a ubiquitin ligase and a target protein, leading to target protein ubiquitination and degradation through the 26S proteasome. <sup>66</sup> This mechanism of chemically induced protein complexation and degradation is emerging as a powerful strategy in the development of probes to

investigate biological processes.<sup>67</sup> Molecular glues also typically overcome the physicochemical limitations of other degraders like proteolysis-targeting chimeras (PROTACs) as they often have lower molecular weight, better cellular permeability, and more favorable pharmacokinetic profiles.<sup>68</sup> This has inspired the discovery of molecular glues from natural products and synthetic molecules and has led to the exploration and development of molecular glues as therapeutic agents.<sup>69</sup>

PCC possibly acts as a molecular glue that causes BRD3 and BRD4 to be degraded by the UPP. The Bt-PCC pulldown in PC-3 cell lysate identified five E3 ligases (TRIM25, UBR4, UBR5, ZNF598, and HUWE1) that interact with PCC, likely through its A ring enone. This interaction may allow one or more of these E3 ligases to ubiquitylate BRD3 and BRD4 and target them for degradation by the 26S proteasome. It is unknown if the PCC A ring enone acts as a Michael acceptor and interacts with an E3 ligase in a covalent manner. A covalent interaction would likely perturb the ability for one PCC molecule to degrade multiple BET proteins and hinder the catalytic degradation typically associated with molecular glues and other small-molecule degraders. The A ring Michael acceptor of PCC may also form a reversible covalent interaction with an E3 ligase or otherwise orient the PCC A ring for more effective E3 ligase engagement. The exact mechanism of BET degradation by PCC in multiple cancer cell types remains to be elucidated, and the relationship between the A ring enone and efficacy in ARnegative PC cells remains unknown. This connection will be further explored in future studies. The possibility for BET degraders to overcome resistance mechanisms that plague current PC therapies, the rise in examination of molecular glues as chemical probes and therapeutic agents, and BET inhibitor development shifting toward molecules with interesting BETselectivity profiles makes PCC a compound worthy of further investigation for PC treatment and as a probe for studying selective BET inhibition and degradation.

## **■ EXPERIMENTAL SECTION**

**Protein Expression for NMR Experiments.** All BDs<sup>22</sup> were subcloned into a Pet23a vector to create a His<sub>6</sub>-BD construct. The plasmid was transformed into T7 Express cells and uniformly [ $^{13}$ C,  $^{15}$ N]-labeled BRD3-BD1 was prepared as follows:  $^{70}$ 1 L cultures were grown in LB at 37 °C to an OD<sub>600</sub> of 0.7 and pelleted by a 10 min centrifugation at 5488g. Cells were then washed and pelleted using an M9 salt solution, excluding all nitrogen and carbon sources. The cell pellet was resuspended in isotopically labeled  $^{13}$ C-Glucose (U-13C6, 99%, Cambridge Isotope Laboratories) (4 g/L),  $^{15}$ NH<sub>4</sub>Cl (99%, Cambridge Isotope Laboratories) (1 g/L) M9 minimal media and then incubated with shaking at 37 °C for 1 h to allow the recovery of growth and clearance of unlabeled metabolites. Cultures were transferred to 16 °C, and protein expression was induced by addition of IPTG to a concentration of 100  $\mu$ M. After a 16 h induction period, the cells were harvested by centrifugation.

**Protein Purification.** Harvested cell pellets were resuspended in ice-cold lysis buffer (50 mM HEPES pH 7.5, 500 mM NaCl, 5% glycerol, 0.5 mM TCEP) and lysed by high-pressure cell homogenization (Microfluidics LM10 Microfluidizer). The bacterial lysate was clarified by centrifugation at 26,895g for 40 min at 4 °C. The supernatant was loaded onto a high-density cobalt resin (GoldBio) column equilibrated with lysis buffer. The His<sub>6</sub>-tagged protein was eluted with lysis buffer and a gradient of increasing imidazole concentration. Fractions containing BRD protein were pooled, TEV protease was added to remove the His<sub>6</sub>-tag, and protein was then removed from dialysis, incubated with Ni-NTA Agarose resin (Qiagen) equilibrated with lysis buffer, and poured through a gravity column to recapture any remaining His<sub>6</sub>-tagged protein. Protein was then

concentrated with Pierce Protein Concentrators (Thermo Scientific) and further purified by size exclusion chromatography (HiLoad 26/600, Superdex 75 pg) equilibrated in NMR buffer (20 mM Tris (pH 7.0), 100 mM NaCl, and 1 mM DTT). Fractions containing pure protein were collected and concentrated with Pierce Protein Concentrators (Thermo Scientific), centrifuged at 10,000g for 10 min at 4  $^{\circ}\mathrm{C}$  to remove debris, flash frozen in liquid nitrogen, and stored at  $-80~^{\circ}\mathrm{C}$ .

BROMOscan Bromodomain Profiling and BromoKdELECT Dose Responses. BROMOscan bromodomain profiling was provided by Eurofins DiscoverX Corp. (San Diego, CA, USA, http://discoverx.com). BROMOscan and BromoKdELECT employ a proprietary ligand binding site-directed competition assay to quantitatively measure interactions between test compounds and bromodomains.

**AlphaScreen.** Four microliters of His-BRD protein post size exclusion chromatography (20–500 nM) in 50 mM HEPES (pH 7.5), 100 mM NaCl, 0.5 mM TCEP, 0.1% BSA, 0.05% Tween-20 was added to 4  $\mu$ L of serially diluted JQ1 or PCC in white low-volume 384-well plates (Greiner 784904) and incubated at room temperature for 30 min. Next, 4  $\mu$ L of biotinylated peptide, H4K5acK8acK12acK16ac (EpiCypher 12-0034), was added (in equal concentration to BRD protein) and incubated for 30 min. Four microliters each of donor (25  $\mu$ g/mL) and acceptor beads (25  $\mu$ g/mL) was added under subdued lighting and incubated in the dark for at least 1 h at room temperature before recording the AlphaScreen signal using an Enspire Alpha plate reader (PerkinElmer). Triplicate data were exported to GraphPad Prism Version 5 for curve fitting with error reported as SEM.

**Protein Thermal Shift Assay.** Protein thermal shift experiments were performed on a Lightcycler 480 II (Roche Molecular Systems) using 96-well PCR plates (USA Scientific 1402-9990) with or without compound (DMSO-matched) in a total volume of 40  $\mu$ L. Thermal shifts were visualized by monitoring the 465 nm/590 nm excitation/emission signal of 1:1000 diluted Sypro Orange (Invitrogen S6650) fluorescence probe, 10  $\mu$ M BRD protein (50 mM HEPES, 500 mM NaCl pH 7.5 buffer), and 50  $\mu$ M compound over a gradient from 20 to 85 °C with 20 acquisitions per °C at a ramp rate of 0.03 °C/s. The observed thermal shift was defined as the midpoint transition between fluorescent maxima/minima at least in three independent experiments. Observed thermal shifts were plotted using GraphPad Prism Version 5 with thermal shifts and SEM reported in °C.

Microscale Thermophoresis. His<sub>6</sub>-BRD protein (80 nM) post size-exclusion chromatography in PBST (0.05% Tween-20) was incubated 1:1 with 10 nM second generation Red-tris-NTA (Nanotemper, MO-LO18) in PBST at room temperature for 30 min prior to centrifugation at 16,179g for 10 min at 4 °C. Labeled BRD protein was aliquoted and incubated with an equivalent volume of serially diluted compound. The mixture was transferred to capillaries (Nanotemper MO-K022) with thermophoresis readouts being captured at 40% LED/MST power using a Monolith NT.115Pico (Nanotemper) instrument. Triplicate data was analyzed using MO Affinity Analysis software (Nanotemper) and exported to GraphPad Prism Version 5 for curve fitting with error reported as SEM.

NMR Spectroscopy.  $^{13}$ C, $^{15}$ N-BRD3-BD1 used for NMR was concentrated to 350  $\mu$ M in NMR buffer. All samples contained 10% D $_2$ O and 0.8%  $d_6$ -DMSO without (apo) or with 400  $\mu$ M PCC. NMR data of BRD3-BD1 were collected at 298 K on a Bruker Avance NEO 600 MHz spectrometer equipped with a TCI HCN z-gradient cryoprobe. Spectra collected were: 2D  $^{15}$ N-HSQC, 2D  $^{13}$ C-HSQC, 3D HNCACB, 3D CBCA(CO)NH, 3D HN(CO)CA, 3D HNCA, 3D HNCO (apo only), and 3D (H)C(CO)NNH-TOCSY (PCC-bound only).  $^{71,72}$  Spectra were processed using TopSpin 4.0 (Bruker). Backbone assignments were completed for apo BRD3-BD1 and PCC bound BRD3-BD1 using NMRFAM-SPARKY $^{73}$  and validated using I-PINE.  $^{74}$  All assignments were submitted to the BMRB (apo, 50801; PCC-bound, 50802).

Crystallization, X-ray Diffraction Data Collection, Structure Solution, and Refinement of the BRD3-BD1/PCC Cocrystal Structure. BRD3-BD1 crystallization experiments were performed by sitting drop vapor diffusion with 17 mg/mL protein in SWISSCI MRC 2 96-well crystallization plates. A Crystal Phoenix dispenser (ARI) was

used to dispense 100 nL of precipitant drops into each well to be combined with either a 100 or 200 nL of protein drop to form each crystallization reaction. Each reaction chamber was sealed and equilibrated against 50  $\mu$ L of precipitant. The precipitant contained 0.2 M ammonium chloride, 10 mM CaCl<sub>2</sub>, 50 mM Tris—HCl (pH 8.5), and 30% w/v polyethylene glycol 4000. Crystal plates were stored in a Phoenix Rigaku Crystalmation system at 293 K and imaged. Crystals that appeared white under UV light were selected for freezing. Crystals 20–100  $\mu$ m in size were taken directly out of the 96-well plate with premounted nylon loops and flash cooled in liquid nitrogen.

X-ray diffraction experiments were carried out at the Structural Biology Center 19-ID beamline at the Advanced Photon Source, Argonne National Laboratory. Crystals were mounted at 100 K and exposed with a microfocus X-ray beam at 0.979 angstrom wavelength. The Pilatus detector was at a 400 mm distance. Each image was exposed for 0.2 s with an oscillation of 0.2 degrees. The complete dataset spanned 900 images with a total wedge size of 180 degrees.

The X-ray data were processed with XDS<sup>75</sup> and merged and scaled with Aimless from the ccp4i<sup>76</sup> package. The phase was determined by molecular replacement (MR) with Phaser,<sup>77</sup> and data processing progressed as described previously.<sup>78,79</sup> The initial model for MR was the apoprotein from PDB: 3S91. Further modeling to fit missing residues as far as possible on the N terminus of the protein backbone was completed manually in Coot.<sup>80</sup> The ligand was introduced in SMILES notation by the JLigand program from the ccp4i<sup>76</sup> suite. The combined model of protein and ligand was refined by Phenix<sup>81</sup> and further checked in Coot for validity. The refined model (PDB: 7R8R) has a 1.80 Å resolution with R/R-free of 0.2002/0.2425 (Table 1).

Crystallization, X-ray Diffraction Data Collection, Structure Solution, and Refinement of the BRD3-BD2/PCC Cocrystal Structure. Crystallization proceeded using the hanging drop vapor diffusion method. Crystals appeared in 48 h with 10 mg/mL BRD3-BD2 and 1.2-fold molar excess PCC in a 1:1 ratio with 0.2 M sodium chloride, 0.1 M Bis-Tris (pH 5.5), and 25% w/v polyethylene glycol 3350 at 24 °C. For data collection, crystals were harvested and exchanged into 0.2 M sodium chloride, 0.1 M Bis-Tris (pH 5.5), 25%  $\mbox{w/v}$  polyethylene glycol 3350, and 30% glycerol and then flash-frozen in liquid nitrogen. X-ray diffraction data collection proceeded at SSRL BL 9-2 using Blu-Ice software.<sup>82</sup> Data processing, including integration, scaling, and merging, was performed with XDS<sup>83,84</sup> and SCALA.<sup>85</sup>, Structure solution was performed using molecular replacement in PHASER<sup>87</sup> within the PHENIX software suite,<sup>88</sup> and so was searching for BRD3-BD2 from the prior apo structure 2001.14 The correct solution was ascertained by the formation of a single domain copy as well as final refinement statistics and was also the highest solution in the molecular replacement. Structure building and refinement proceeded through an interactive process and COOT, 80,89 ligand coordinates and restraints using ELBOW<sup>90</sup> of PHENIX, and refinement using PHENIX. <sup>91–93</sup> The refined model (PDB: 7S3P) has a 2.89 Å resolution with an R/R-free of 0.2056/0.2406 (Table 1).

**Fluorescence Polarization Assay.** Fluorescence polarization experiments were performed in black low-volume 384-well plates (Greiner 784706). Each well received a 5  $\mu$ L mixture of 14 (4 nM) and BRD protein (20–400 nM) in FP buffer (50 mM HEPES (pH 7.4), 150 mM NaCl, 0.5 mM TCEP, and 0.05% Tween-20). DMSO or serially diluted compound (15  $\mu$ L, DMSO-matched) in FP buffer was added. Plates were incubated prior to obtaining signal (485 nm/535 nm excitation/emission) on a SpectraMax iD5 plate reader (Molecular Devices). Fluorescence polarization was determined after adjusting the G-factor to zero for polarization of 14 alone in DMSO-matched FP buffer. Triplicate data were exported to GraphPad Prism Version 5 for curve fitting with error reported as SEM.

qRT-PCR. VCaP cells were grown to 50% confluence, treated for 16 h with DMSO, JQ1, or PCC, and then harvested. A Qiagen RNeasy kit (74104) was used to isolate total RNA and cDNA synthesized from 1  $\mu$ g of isolated RNA using SuperScript III First-Strand Synthesis Supermix (Thermo 18080400). qPCRs were performed on a Lightcycler 480 II (Roche Molecular Systems) using 96-well PCR plates (USA Scientific 1402–9990) in triplicate using PowerUp SYBR Green Master Mix (Applied Biosystems A25741). The  $\Delta\Delta$ Ct method

was used to quantify target mRNA expression (normalized to GAPDH expression). Primer sequences are as follows: BRD2 F: 5' CTACGTAAGAAACCCCCGGAAG; BRD2 R: 5' GCTTTTTCTCCAAAGCCAGTT; BRD3 F: 5' CCTCAGGGAGATGCTATCCA; BRD3 R: 5' ATGTCGTGGTAGTCG TGCAG; BRD4 F: 5' AGCAGCAACAGCAATGTGAG; BRD4 R: 5' GCTTGCACTTGTCCTCTTCC; ERG F: 5' CGCAGAGTTATCGTGCCAGCAGAT; ERG R: 5' CCATATTCTTTCACCGCCCACTCC; PSA F: 5' ACGCTGGACAGGGGGCAAAAG; PSA R: 5' GGGCAGGGCACATGGTTCACT; TMPRSS2 F: 5' CAGGAGTGTACGGGAATGTGATGGT; TMPRSS2 R: 5' GATTAGCCGTCTGCCCTCATTTGT; AR F: 5' CAGTGGATGGGCTGAAAAAT; AR R: 5' GGAGCTTGGTGAGCTGGTAG; GAPDH F: 5' TGCACCACCACACTGCTTAGC; GAPDH R: 5' GGCATGGACTGTG GTCATGAG.

Immunoblotting. Fifty percent confluent MDA-MB-231 or PC-3 (University of Arizona Cancer Cell Repository) cells grown in DMEM, 10% FBS, and 1× pen/strep were treated overnight with compound (or for time periods as indicated by timecourse), washed once with PBS, trypsinized, and collected by centrifugation (3000g for 10 minutes) followed by lysis with RIPA lysis buffer supplemented with 1 mM PMSF, 5 mM EDTA, and 1× Halt protease inhibitor cocktail (Thermo Scientific, #78430). Lysate was centrifuged (22,240g for 30 minutes) and supernatant collected for analysis by immunoblotting. Primary antibodies used in this study include: BRD2 (Cell Signaling, D89B4), BRD3 (Santa Cruz, sc-81202), BRD4 (Cell Signaling, E2A7X), GAPDH (Santa Cruz, sc-32233). Secondary HRP antibodies were obtained from Sigma (A-9044 and A-0545). Luminescence (Supersignal West Femto, Thermo Scientific, #34096) was detected using an Azure Biosystems 600 imager. DC50 values were determined by gel band densitometry analysis performed using ImageJ 1.53t (NIH).

Cell Viability Assay. Cell viability was measured in a 96-well microplate format by MTS dye assay (Promega, Madison, WI, USA). Compounds were tested against metastatic human prostate adenocarcinoma (VCaP), androgen-sensitive human prostate adenocarcinoma (LNCaP), androgen-resistant human prostate adenocarcinoma (22Rv1), human androgen receptor-positive prostate adenocarcinoma (DU-145), androgen-insensitive human prostate adenocarcinoma (PC-3), human foreskin fibroblast cells (HFF), and human-diploid lung fibroblast cells (WI-38). Serial dilutions of compounds in DMSO, negative control (DMSO), or positive control (doxorubicin) were added to triplicate wells. After 72 h of incubation, cell viability was determined by the addition of CellTiter 96 AQueous One Solution Cell Proliferation Assay reagent (MTS), plates were incubated for 2 h, and then absorbance (A) at 490 nM was measured. Cytotoxicity was calculated with the following formula: % cytotoxicity =  $[(A_{medium} - A_{medium})]$  $A_{\text{treatment}}/A_{\text{medium}})] \times 100$ . The EC<sub>50</sub> values and standard deviations (±) were determined using Microsoft Excel software from doseresponse curves obtained from at least three independent experiments.

Pulldown and LC-MS/MS. Bt-PCC pulldown was performed as previously described. 40 LC–MS/MS analysis was carried out using a Q Exactive Plus mass spectrometer (Thermo Fisher Scientific, San Jose, CA) equipped with an Easy Spray nanoESI source. Peptides were eluted from an Acclaim Pepmap 100 trap column (75  $\mu$ m ID  $\times$  2 cm, Thermo Scientific) onto an Acclaim PepMap RSLC analytical column (75  $\mu$ m ID × 25 cm, Thermo Scientific) using a 3–38% gradient of solvent B (90% acetonitrile and 0.1% formic acid) over 35 min, 38-74% solvent B over 10 min, and 74-100% of solvent B over 5 min, then held with 100% solvent B for 10 min, and finally returned to 3% solvent B for 10 min. Solvent A consisted of water and 0.1% formic acid. Flow rates were 300 nL/min using a Thermo Scientific EASY-nLC 1200 System (Thermo Scientific). Data-dependent scanning was performed by Xcalibur v 4.0.27.19 software using a survey scan at 70,000 resolution, scanning mass/charge (m/z) 360-1600, automatic gain control (AGC) target of 1e5, and a maximum injection time (IT) of 65 ms followed by higher-energy collisional dissociation (HCD) tandem mass spectrometry (MS/MS) at 27 nce (normalized collision energy) of the 10 most intense ions at a resolution of 17,500, an isolation width of 1.5 m/z, an AGC of 1e5 and a maximum IT of 65 ms. Dynamic exclusion was set to place any selected m/z on an exclusion list for 20 s

after a single MS/MS. Ions of charge states +1, 7, 8, >8, and unassigned were excluded from MS/MS, as were isotopes. All MS/MS spectra were searched using Thermo Proteome Discoverer v 2.4 (Thermo Fisher Scientific) considering fully tryptic peptides with up to two missed cleavage sites. Variable modifications considered during the search included methionine oxidation (15.995 Da) and cysteine carbamidomethylation (57.021 Da). Proteins were identified at 99% confidence with XCorr score cut-offs (Qian et al., 2005) as determined by a reversed database search. The protein and peptide identification results were visualized with Scaffold Q + S v 5.0.1 (Proteome Software Inc., Portland OR), a program that relies on various search engine results (i.e., Sequest, X!Tandem, MASCOT) and uses Bayesian statistics to reliably identify more spectra. Protein identifications were accepted that passed a minimum of two peptides identified at a 0.1% peptide false discovery rate and 90–99.9% protein confidence.

Chemistry. All reagents used for chemical transformations were purchased from Sigma Aldrich (St. Louis, MO, USA) and Fisher Scientific (Pittsburgh, PA, USA). All solvents used were distilled before use. The progress of all reactions was monitored by thin-layer chromatography (TLC) on silica gel 60 F<sub>254</sub> plates (Merck, Darmstadt, Germany), and spots were visualized under UV and sprayed with a solution of anisaldehyde in H2SO4 and HOAc followed by heating. Column chromatographic separations were performed on silica gel 40  $\mu$ m flash chromatography packing (J. T. Baker, Jackson, TN, USA). Preparative HPLC was performed on a Waters Delta Prep 4000 preparative chromatography system equipped with a Waters 996 photodiode array detector and a Waters Prep LC controller utilizing Empower Pro software and using a RP column (Kromasil KR100-7-C18; 250 mm × 20 mm) with a flow rate of 8.0 mL/min; chromatograms were acquired at 254 and 270 nm. All compounds used for biological evaluation are >95% pure by HPLC. 1D and 2D NMR spectra were recorded in CDCl<sub>3</sub> or CDCl<sub>3</sub> + CD<sub>3</sub>OD with a Bruker AVANCE III instrument at 400 MHz for <sup>1</sup>H NMR and 100 MHz for  $^{13}\mathrm{C}$  NMR using residual CHCl $_3$  as the internal standard. The chemical shift  $(\delta)$  values are given in parts per million (ppm) and the coupling constants (J values) are in Hz. High-resolution mass spectra were recorded on an Agilent G6224A TOF mass spectrometer. Lowresolution mass spectra were recorded on a Waters autopurification system equipped with an Acquity QDa detector.

Isolation of Naturally Occurring Withanolides. Withanolide E (1) and 24,25-dihydrowithanolide E (7) were isolated from aerial parts of aeroponically cultivated *P. peruviana*. Physachenolide C (PCC), Physachenolide D (2), 18-acetoxy-17-epi-withanolide K (3), and 15 $\alpha$ -acetoxyphysachenolide C (6) were isolated from aerial parts of aeroponically cultivated *P. crassifolia*. 45,46 28-Hydroxyphysachenolide C (8) was obtained from aeroponically grown *P. coztomatl*. Withaferin A (9) was isolated from aerial parts of aeroponically cultivated *W. somnifera*. 47

Preparation of Withanolide Analogues. 24α,25α-Epoxyphysachenolide C (4), 5,6-epi-physachenolide C (5), and 2,3-dihydrophysachenolide C (13) were prepared as described previously. Withanolide analogues 10–12 and physachenolide C (PCC)-NHS-fluorescein conjugate 14 were prepared as described below.

(24R,25R)-2,3,24,25-Tetrahydrophysachenolide C (10). To a solution of physachenolide C (PCC) (20.0 mg, 36.8  $\mu$ mol) in anhydrous ethanol (2.0 mL) was added 5% Pt on C (50.0 mg) and stirred under an atmosphere of H<sub>2</sub> for 36 h (TLC controlled). The reaction mixture was then filtered, the filtrate was evaporated under reduced pressure, and the residue (17.4 mg) was chromatographed over a column of silica gel (1.0 g) made up in MeOH/CH<sub>2</sub>Cl<sub>2</sub> (2:98) and eluted with MeOH/CH<sub>2</sub>Cl<sub>2</sub> (2:98). Middle fractions were combined (according to TLC profile) and rechromatographed over a column of silica gel (0.5 g) made up in hexanes/isopropanol (9:1) and eluted with hexanes/isopropanol (9:1) followed by hexanes/isopropanol (8:2). Middle fractions eluted with hexanes/isopropanol (9:1) were combined to give (24R,25R)-2,3,24,25-tetrahydrophysachenolide C [(20S,22R,24S,25S)-18-acetoxy-5 $\beta$ ,6 $\beta$ -epoxy-2,3,24,25-tetrahydro- $14\alpha$ ,  $17\beta$ , 20-trihydroxy-1-oxowithanolide (10, 2.8 mg, 14%) as a white amorphous solid; <sup>1</sup>H NMR (400 MHz, CDCl<sub>3</sub>):  $\delta$  4.84 (1H, dd, J = 11.5, 3.5 Hz, H-22), 4.33 (1H, d, J = 11.5 Hz, Ha-18), 4.27 (1H, d, J =

11.5 Hz, Hb-18), 3.17 (1H, t, I = 1.4 Hz, H-6), 2.71 (1H, m, Ha-2), 2.68 (1H, m, H-24), 2.62 (1H, m, Ha-16), 2.25 (1H, m, Hb-2), 2.21 (1H, m, Ha-23), 2.18 (1H, m, Ha-12), 2.16 (1H, m, H-25), 2.05 (3H, s, COCH<sub>3</sub>), 2.02 (2H, m, H<sub>2</sub>-7), 1.97 (1H, m, Ha-4), 1.84 (3H, m, H<sub>2</sub>-3, H-9), 1.73 (1H, H-8), 1.70 (1H, m, Hb-12), 1.66 (1H, m, Ha-15), 1.55 (2H, m, Hb-15, Hb-16), 1.44 (1H, m, Hb-23), 1.33 (3H, s, H<sub>3</sub>-21), 1.30 (2H, m, H<sub>2</sub>-11), 1.21 (1H, m, Hb-4), 1.14 (3H, d, J = 7.2 Hz, H<sub>3</sub>-27),1.13 (3H, s, H<sub>3</sub>-19), 0.91 (3H, d, J = 6.7 Hz, H<sub>3</sub>-28); <sup>13</sup>C NMR (100 MHz, CDCl<sub>3</sub>):  $\delta$  213.3 (C, C-1), 174.8 (C, C-26), 169.8 (C, OCOCH<sub>3</sub>), 88.0 (C, C-17), 81.7 (C, C-14), 81.3 (CH, C-22), 79.4 (C, C-20), 64.9 (CH<sub>2</sub>, C-18), 64.3 (C, C-5), 60.9 (CH, C-6), 57.7 (C, C-13), 52.4 (C, C-10), 38.5 (CH, C-24), 37.8 (CH<sub>2</sub>, C-16), 35.6 (CH, C-9), 34.8 (CH<sub>2</sub>, C-2), 33.6 (CH, C-8), 32.9 (CH<sub>2</sub>, C-15), 31.7 (CH<sub>2</sub>, C-23), 30.1 (CH<sub>2</sub>, C-4), 29.7 (CH, C-25), 26.6 (CH<sub>2</sub>, C-7), 25.2 (CH<sub>2</sub>, C-12), 21.4 (CH<sub>2</sub>, C-11), 21.2 (CH<sub>3</sub>, OCOCH<sub>3</sub>), 18.5 (CH<sub>3</sub>, C-21), 18.2 (CH<sub>3</sub>, C-28), 17.8 (CH<sub>2</sub>, C-3), 12.6 (CH<sub>3</sub>, C-19), 12.0 (CH<sub>3</sub>, C-27); HRMS (ESI<sup>+</sup>): calcd for C<sub>30</sub>H<sub>48</sub>NO<sub>9</sub> [M + NH<sub>4</sub>]<sup>+</sup> 566.3329, found

2,3-Dihydro-3 $\alpha$ -hydroxyphysachenolide D (15). To a solution of physachenolide D (2, 100.0 mg, 189.4  $\mu$ mol), bis(pinacolato)diboron  $(76.0 \text{ mg}, 300.0 \,\mu\text{mol})$ , CuCl<sub>2</sub>  $(54.0 \text{ mg}, 409.0 \,\mu\text{mol})$ , and Et<sub>3</sub>N  $(150.0 \,\mu\text{mol})$  $\mu$ L, 1.04 mmol) in THF (5.0 mL) was added a solution of CuCl<sub>2</sub> in H<sub>2</sub>O (1.72 mM, 10.0 mL) and stirred at 25 °C for 10 min (until the starting material disappeared as monitored by TLC). To this solution was added NaBO<sub>3</sub>.4H<sub>2</sub>O (200.0 mg), and the solution was stirred at 25 °C. After 30 min, the reaction mixture was diluted with H<sub>2</sub>O (15.0 mL) and extracted with EtOAc ( $3 \times 50.0$  mL). The combined EtOAc layer was washed with  $H_2O$  (3 × 20.0 mL), dried over anhydrous  $Na_2SO_4$ , and evaporated under reduced pressure. The residue (158.0 mg) thus obtained was chromatographed over a column of silica gel (3.0 g) made up in CH<sub>2</sub>Cl<sub>2</sub> and eluted with MeOH/CH<sub>2</sub>Cl<sub>2</sub> (2:98) followed by MeOH/CH<sub>2</sub>Cl<sub>2</sub> (4:96). Fractions eluted with MeOH/CH<sub>2</sub>Cl<sub>2</sub> (4:96) were combined to give 2,3-dihydro- $3\alpha$ -hydroxyphysachenolide D [(20S,22R)-18-acetoxy-2,3-dihydro- $3\alpha$ ,14 $\alpha$ ,17 $\beta$ ,20-tetrahydroxy-1-oxowitha-5,24-dienolide] (15, 101.3 mg, 98%) as an amorphous solid. <sup>1</sup>H NMR (400 MHz, CDCl<sub>3</sub>):  $\delta$  5.62 (1H, d, J = 5.1 Hz, H-6), 4.86 (1H, dd, J = 11.2, 6.6 Hz, H-22), 4.43 (1H, d, J = 11.6 Hz, Ha-18), 4.32 (1H, d, J = 11.6 Hz, Hb-18), 4.25 (1H, brt, J = 4.0 Hz, H-3), 2.83 (1H, dd, J =13.4,3.9 Hz, Ha-2), 2.78 (1H, m, Ha-16), 2.50 (2H, m, H<sub>2</sub>-23), 2.43 (1H, m, Hb-2), 2.39 (1H, m, H-9), 2.34 (1H, m, Ha-12), 2.28 (1H, m, Ha-7), 2.25 (1H, m, Hb-16), 2.08 (3H, s, OCOCH<sub>3</sub>), 1.92 (3H, s, H<sub>3</sub>-28), 1.86 (3H, s, H<sub>3</sub>-27), 1.83 (1H, m, Hb-7), 1.81 (1H, m, Ha-11), 1.76 (1H, m, H-8), 1.73 (1H, m, Hb-12), 1.66–1.57 (4H, m, H<sub>2</sub>-4 and H<sub>2</sub>-15), 1.27 (1H, m, Hb-11), 1.40 (3H, s, H<sub>3</sub>-21), 1.24 (3H, s, H<sub>3</sub>-19);  $^{13}$ C NMR (100 MHz, CDCl<sub>3</sub>):  $\delta$  212.3 (C, C-1), 170.0 (C, OCOCH<sub>3</sub>), 165.9 (C, C-26), 149.8 (C, C-24), 136.0 (C, C-5), 127.1 (CH, C-6), 121.8 (C, C-25), 88.3 (C, C-17), 81.4 (C, C-14), 79.9 (CH, C-22), 78.6 (CH, C-20), 67.8 (CH, C-3), 65.1 (CH<sub>2</sub>, C-18), 57.6 (C, C-13), 53.8 (C, C-10), 46.5 (CH<sub>2</sub>, C-2), 39.3 (CH<sub>2</sub>, C-16), 36.3 (CH, C-8), 35.3 (CH, C-9), 32.9 (CH<sub>2</sub>, C-4), 32.8 (CH<sub>2</sub>, C-15), 26.0 (CH<sub>2</sub>, C-7), 25.7 (CH<sub>2</sub>, C-12), 21.9 (CH<sub>2</sub>, C-11), 21.3 (CH<sub>3</sub>, OCOCH<sub>3</sub>), 20.7 (CH<sub>3</sub>, C-28), 19.2 (CH<sub>3</sub>, C-21), 18.6 (CH<sub>3</sub>, C-19), 12.4 (CH<sub>3</sub>, C-27); HRMS (ESI<sup>+</sup>): calcd for  $C_{30}H_{46}NO_9[M + NH_4]^+$  564.3173, found 564.3164.

2,3-Dihydro-3 $\alpha$ -O-tert-butyldimethylsilylphysachenolide D (16). To a solution of 15 (50 mg, 91.6  $\mu$ mol) in anhydrous N,Ndimethylformamide (DMF, 8.0 mL) was added 4-pyrrolidinopyridine (4-pp, 174.5 mg, 1.18 mmol), and tertiary butyldimethysilylchloride (t-BDMSCl, 141.5 mg, 0.94 mmol) and stirred at 60 °C. After 16 h, the reaction mixture was diluted with EtOAc (100.0 mL), washed with brine (5 × 20 mL), dried over anhydrous Na<sub>2</sub>SO<sub>4</sub>, and evaporated under reduced pressure. Residue (189.9 mg) was then chromatographed over a column of silica gel (4.0 g) made up in hexanes/EtOAc (1:1) and eluted with hexanes/EtOAc (1:1) followed by hexanes/ EtOAc (3:7). Fractions eluted with hexanes/EtOAc (3:7) were combined to give 2,3-dihydro-3α-O-tert-butyldimethylsilylphysachenolide D [(20S,22R)-18-acetoxy-2,3-dihydro-3 $\alpha$ -O-tert-butyldimethylsilyl-14 $\alpha$ ,17 $\beta$ ,20-trihydroxy-1-oxowitha-5,24-dienolide] (16, 59.8 mg, 99%) as an amorphous solid. <sup>1</sup>H NMR (400 MHz, CDCl<sub>3</sub>):  $\delta$  5.48 (1H, d, J = 4.7 Hz, H-6), 4.85 (1H, dd, J = 10.7, 7.7 Hz, H-22), 4.41 (1H, d, J $= 12.0 \,\mathrm{Hz}$ , Ha-18), 4.33 (1H, d,  $J = 12.0 \,\mathrm{Hz}$ , Hb-18), 4.18 (1H, m, H-3),

2.67 (1H, dd, I = 12.8, 3.9 Hz, Ha-2), 2.66 (1H, m, Ha-16), 2.62 (1H, m, Ha-4), 2.52–2.50 (2H, m, H<sub>2</sub>-23), 2.34 (2H, m, Hb-2, Ha-7), 2.33 (1H, m, H-9), 2.25 (1H, m, Ha-12), 2.09 (1H, dt, J = 14.1, 2.2 Hz, Hb-12)4), 2.06 (3H, s, OCOCH<sub>3</sub>), 1.91 (3H, s, H<sub>3</sub>-28), 1.85 (3H, s, H<sub>3</sub>-27), 1.80 (2H, m, Hb-7, Ha-11), 1.73 (2H, m, H-8, Hb-12), 1.64-1.58 (2H, m, H<sub>2</sub>-15), 1.51 (1H, m, Hb-16), 1.39 (3H, s, H<sub>3</sub>-21), 1.27 (1H, m, Hb-11),  $\overline{1.18}$  (3H, s, H<sub>3</sub>-19), 0.80 [9H, C-(CH<sub>3</sub>)<sub>3</sub>], -0.03 (6H, 2 × Si-CH<sub>3</sub>);  $^{13}$ C NMR (100 MHz, CDCl<sub>3</sub>):  $\delta$  212.3 (C, C-1), 170.4 (C, OCOCH<sub>3</sub>), 165.8 (C, C-26), 149.8 (C, C-24), 136.7 (C, C-5), 125.2 (CH, C-6), 121.7 (C, C-25), 88.2 (C, C-17), 81.3 (C, C-14), 79.8 (CH, C-22), 78.7 (CH, C-20), 68.3 (CH, C-3), 65.1 (CH<sub>2</sub>, C-18), 57.6 (C, C-13), 53.3 (C, C-10), 46.9 (CH<sub>2</sub>, C-2), 40.2 (CH<sub>2</sub>, C-4), 38.0 (CH<sub>2</sub>, C-16), 36.4 (CH, C-8), 35.4 (CH, C-9), 33.7 (CH<sub>2</sub>, C-23), 32.7 (CH<sub>2</sub>, C-15), 25.9 (CH<sub>2</sub>, C-12), 25.6 [CH<sub>3</sub>, C-(CH<sub>3</sub>)<sub>3</sub>], 25.5 (CH<sub>2</sub>, C-7), 21.9 (CH<sub>2</sub>, C-11), 21.3 (CH<sub>3</sub>, OCOCH<sub>3</sub>), 20.6 (CH<sub>3</sub>, C-28), 19.3 (CH<sub>3</sub>, C-21), 18.6 (CH<sub>3</sub>, C-19), 17.9 [C, C-(CH<sub>3</sub>)<sub>3</sub>], 12.4 (CH<sub>3</sub>, C-27), 4.8 (CH<sub>3</sub>, Si-CH<sub>3</sub>), 4.9 (CH<sub>3</sub>, Si-CH<sub>3</sub>); HRMS (ESI<sup>+</sup>): calcd for C<sub>36</sub>H<sub>56</sub>NaO<sub>9</sub>Si [M + Na]+ 683.3581, found 683.3586.

2,3-Dihydro-3 $\alpha$ -O-tert-butyldimethylsilylphysachenolide C (17). To a solution of **16** (40.0 mg, 60.6  $\mu$ mol) in CH<sub>2</sub>Cl<sub>2</sub> (2.0 mL) at 25 °C was added meta-chloroperbenzoic acid (m-CPBA, 77%) (30.0 mg, 134.3  $\mu$ mol) and stirred at 25 °C for 3 h (TLC controlled). The reaction mixture was then concentrated and chromatographed over a column of silica gel (2.0 g) made up in toluene/EtOAc (4:6) and eluted with toluene/EtOAc (4:6) to give 2,3-dihydro-3α-O-tert-butyldimethylsilylphysachenolide C  $[(20S,22R)-18-acetoxy-2,3-dihydro-3\alpha-O$ *tert*-butyldimethylsilyl-5 $\beta$ ,6 $\beta$ -epoxy-14 $\alpha$ ,17 $\beta$ ,20-trihydroxy-1-oxowitha-24-enolide] (17, 27.6 mg, 67%) as an amorphous solid. <sup>1</sup>H NMR  $(400 \text{ MHz}, \text{CDCl}_3)$ :  $\delta 4.83 (1\text{H}, \text{dd}, J = 9.7, 6.7 \text{ Hz}, \text{H-}22), 4.34 (1\text{H}, \text{d}, \text{J})$ J = 11.2 Hz, Ha-18), 4.24 (1H, d, J = 11.2 Hz, Hb-18), 4.18 (1H, m, H-3), 3.27 (1H, brs, H-6), 2.66 (3H, m, H<sub>2</sub>-2, Ha-16), 2.50–2.48 (2H, m,  $H_2$ -23), 2.21 (1H, dd, J = 14.1, 4.6 Hz,  $H_2$ -4), 2.19 (1H, m,  $H_2$ -12), 2.04 (3H, s, OCOCH<sub>3</sub>), 2.03-1.96 (2H, m, H<sub>2</sub>-7), 1.94 (1H, m, H-9), 1.91 (3H, s, H<sub>3</sub>-28), 1.85 (3H, s, H<sub>3</sub>-27), 1.75 (1H, m, H-8), 1.69 (1H, m, Hb-12), 1.67 (1H, m, Ha-15), 1.56 (1H, m, Hb-15), 1.53 (1H, m, Hb-16), 1.43 (1H, m, Ha-11), 1.38 (3H, s, H<sub>3</sub>-21), 1.29 (1H, brd, *J* = 14.1 Hz, Hb-4), 1.23 (1H, m, Hb-11), 1.12 (3H, s, H<sub>3</sub>-19), 0.82 [9H, s,  $C-(CH_3)_3$ , -0.01 (3H, s, Si-CH<sub>3</sub>), -0.02 (3H, s, Si-CH<sub>3</sub>); <sup>13</sup>C NMR (100 MHz, CDCl<sub>3</sub>): δ 211.0 (C, C-1), 170.1 (C, OCOCH<sub>3</sub>), 165.7 (C, C-26), 149.8 (C, C-24), 121.8 (C, C-25), 88.0 (C, C-17), 81.2 (C, 14), 79.5 (CH, C-22), 78.8 (CH, C-20), 64.8 (CH<sub>2</sub>, C-18), 64.5 (CH, C-3), 62.3 (CH, C-6), 62.2 (C, C-5), 57.5 (C, C-13), 51.9 (C, C-10), 46.2 (CH<sub>2</sub>, C-2), 40.5 (CH<sub>2</sub>, C-4), 38.0 (CH<sub>2</sub>, C-16), 35.4 (CH, C-9), 33.8 (CH<sub>2</sub>, C-23), 33.6 (CH, C-8), 32.9 (CH<sub>2</sub>, C-15), 26.4 (CH<sub>2</sub>, C-7), 25.6 [CH<sub>3</sub>, C-(CH<sub>3</sub>)<sub>3</sub>], 25.2 (CH<sub>2</sub>, C-12), 21.7 (CH<sub>2</sub>, C-11), 21.2 (CH<sub>3</sub>, OCOCH<sub>3</sub>), 20.6 (CH<sub>3</sub>, C-28), 19.2 (CH<sub>3</sub>, C-21), 17.8 [C, C-(CH<sub>3</sub>)<sub>3</sub>], 13.6 (CH<sub>3</sub>, C-19), 12.4 (CH<sub>3</sub>, C-27), -4.9 (CH<sub>3</sub>, Si-CH<sub>3</sub>), -5.0 (CH<sub>3</sub>,  $Si-CH_3$ ); LC/MS (ESI<sup>+</sup>): calcd for  $C_{36}H_{57}O_{10}Si [M + H]^+ 677.4$ , found

2,3,24,25-Tetrahydro-3 $\alpha$ -O-tert-butyldimethylsilylphysachenolide C (18). To a solution of 17 (27.0 mg, 39.8  $\mu$ mol) in EtOH (2.0 mL) was added 10% Pd on C (30.0 mg) and stirred under atmosphere of H<sub>2</sub>. After 24 h (TLC-controlled), the reaction mixture was filtered, the filtrate was evaporated under reduced pressure, and the residue was chromatographed over a column of silica gel (1.0 g) made up in toluene/acetone (8:2) and eluted with toluene/acetone (8:2) to give a mixture of (24R,25R)- 2,3,24,25-tetrahydro-3 $\alpha$ -O-tert-butyldimethylsilylphysachenolide C  $[(20S,22R,24R,25R)-18-acetoxy-5\beta,6\beta-epoxy-$ 2,3,24,25-tetrahydro- $3\alpha$ -*O-tert*-butyldimethylsilyl- $14\alpha$ ,17 $\beta$ ,20-trihydroxy-1-oxowithanolide] and (24S,25S)-2,3,24,25-tetrahydro-3 $\alpha$ -Otert-butyldimethylsilylphysachenolide C [(20S,22R,24S,25S)-18-acetoxy- $5\beta$ , $6\beta$ -epoxy-2,3,24,25-tetrahydro- $3\alpha$ -*O-tert*-butyldimethylsilyl- $14\alpha$ ,  $17\beta$ , 20-trihydroxy-1-oxowithanolide] (18, 5.7 mg, 21%) as an amorphous solid. <sup>1</sup>H NMR (400 MHz, CDCl<sub>3</sub>): δ 5.03 (m, H-22), 4.84 (m, H-22), 4.40-4.25 (m, H<sub>2</sub>-18), 4.20 (m, H-3), 3.27 (brs, H-6), 2.67(m, H<sub>2</sub>-2), 2.50 (m, H-23), 2.05 (s, OCOCH<sub>3</sub>), 2.04 (s, OCOCH<sub>3</sub>), 1.44 (s,  $H_3$ -21), 1.39 (s,  $H_3$ -21), 1.23 (s,  $H_3$ -19), 1.20 (d, J = 7.1 Hz), 1.04 (d, J = 7.1 Hz), 1.01 (d, J = 7.1 Hz), 0.92 (d, J = 7.1 Hz), 0.82 [s, C-1.04 (d, J = 7.1 Hz) $(CH_3)_3$ , -0.02 [s,  $Si(CH_3)_2$ ]; LC/MS (ESI<sup>+</sup>): calcd for  $C_{36}H_{56}NaO_{10}Si [M + Na]^{+} 701.4$ , found 701.4.

2,3,24,25-Tetrahydro-3 $\alpha$ -hydroxyphysachenolide C (19). To a solution of 18 (5.5 mg, 8.1  $\mu$ mol) in tetrahydrofuran (THF, 1.0 mL) at 0 °C was added a solution of tetrabutylammonium fluoride in THF (1.0 M, 15.0  $\mu$ L, 15  $\mu$ mol) and stirred at 0 °C for 30 min (TLC-controlled). Reaction mixture was diluted with EtOAc (15.0 mL), washed with 2 N HCl(0.5 mL),  $H_2O(5 \times 10.0 \text{ mL})$ , dried over anhydrous  $Na_2SO_4$ , and evaporated under reduced pressure. Residue was then separated on prep TLC using MeOH/CH<sub>2</sub>Cl<sub>2</sub> (8:92, R<sub>f</sub> 0.3) as eluant to give a mixture of (24R,25R)-2,3,24,25-tetrahydro-3 $\alpha$ -hydroxyphysachenolide C [(20S,22R,24R,25R)-18-acetoxy-5 $\beta$ ,6 $\beta$ -epoxy-2,3,24,25-tetrahydro- $3\alpha,14\alpha,17\beta,20$ -tetrahydroxy-1-oxowithanolide] and (24S,25S)-2,3,24,25-tetrahydro-3α-hydroxyphysachenolide C [(20S,22R,24S,25S)-18-acetoxy- $5\beta$ , $6\beta$ -epoxy-2,3,24,25-tetrahydro- $3\alpha$ ,  $14\alpha$ ,  $17\beta$ , 20-tetrahydroxy-1-oxowithanolide (19, 4.1 mg, 90%) as an amorphous solid. <sup>1</sup>H NMR (400 MHz, CDCl<sub>3</sub>):  $\delta$  5.03 (m, H-22), 4.84 (m, H-22), 4.40-4.20 (m, H<sub>2</sub>-18), 3.96 (m, H-3), 3.32 (brs, H-6), 2.75 (m, H<sub>2</sub>-2), 2.50 (m, H-23), 2.05 (s, OCOCH<sub>3</sub>), 2.04 (s, OCOCH<sub>3</sub>), 1.43 (s, H<sub>3</sub>-21), 1.34 (s, H<sub>3</sub>-21), 1.23 (s, H<sub>3</sub>-19), 1.20 (d, J = 7.1 Hz), 1.04 (d, J = 7.1 Hz), 1.00 (d, J = 7.1 Hz), 0.95 (d, J = 7.1 Hz), 0.92 (d, J = 7.1 Hz); LC/MS (ESI<sup>+</sup>): LC/MS (ESI<sup>-</sup>): calcd for  $C_{30}H_{41}O_9$  [M-H-H<sub>2</sub>O]<sup>-</sup> 545.3, found 545.3.

(24R,25R)-24,25-Dihydrophysachenolide C (11) and (24S,25S)-24,25-Dihydrophysachenolide C (12). To a solution of 19 (4.0 mg, 7.1 µmol) in anhydrous EtOAc (0.5 mL) was added 4-nitobenzoic acid  $(3.5 \text{ mg}, 20.9 \,\mu\text{mol})$ , DCC  $(4.4 \text{ mg}, 21.3 \,\mu\text{mol})$  and 4-pp  $(ca~0.5 \text{ mg}, 3.4 \,\mu\text{mol})$  $\mu$ mol) and stirred at 25 °C for 4 h. To this solution was then added excess 4-pp (10.0 mg) and stirred at 25 °C for 16 h. The reaction mixture was filtered, and the filtrate was evaporated under reduced pressure to give a crude product mixture (5.6 mg). This was purified by RP-HPLC (CH<sub>3</sub>CN/H<sub>2</sub>O; 4:6,  $t_R$  = 20 min) followed by preparative TLC [hexanes/isopropanol; 8:2 (triple elution)] to give (24R,25R)-24,25-dihydrophysachenolide C [(20S,22R,24R,25R)-18-acetoxy-24,25-dihydro- $5\beta$ ,6 $\beta$ -epoxy- $14\alpha$ ,1 $7\beta$ ,20-trihydroxy-1-oxowitha-2-enolide] (11, 2.6 mg, 67%,  $R_f = 0.59$ ): <sup>1</sup>H NMR (400 MHz, CDCl<sub>3</sub>):  $\delta$  6.81 (1H, ddd, J = 10.0, 6.3, 2.3 Hz, H-3), 6.00 (1H, dd, J = 10.0, 2.9 Hz, H-3)2), 4.88 (1H, dd, *J* = 12.3, 3.8 Hz, H-22), 4.44 (1H, d, *J* = 11.5 Hz, Ha-18), 4.28 (1H, d, *J* = 11.5 Hz, Hb-18), 3.15 (1H, brt, *J* = 2.1 Hz, H-6), 2.93 (1H, dt, J = 18.5, 2.8 Hz, Ha-4), 2.71 (1H, pentet, J = 7.1 Hz, H-25), 2.60 (1H, m, Ha-16), 2.24 (2H, m, Ha-12, Ha-23), 2.20 (1H, m, H-24), 2.10 (1H, m, Ha-11), 2.06 (3H, s, OCOCH<sub>3</sub>), 1.96 (2H, m, H<sub>2</sub>-7), 1.88 (1H, m, H-9), 1.84 (2H, m, Hb-4, H-8), 1.77 (1H, brd, J = 12.9 Hz,Hb-12), 1.64 (1H, m, Ha-15), 1.55 (2H, m, Hb-15, Hb-16), 1.45 (1H, m, Hb-23), 1.42 (1H, m, Hb-11), 1.34 (3H, s, H<sub>3</sub>-21), 1.22 (3H, s, H<sub>3</sub>-19), 1.16 (3H, d, J = 7.1 Hz, H<sub>3</sub>-27), 0.92 (3H, d, J = 7.1 Hz, H<sub>3</sub>-28); <sup>13</sup>C NMR (100 MHz, CDCl<sub>3</sub>):  $\delta$  203.0 (C, C-1), 174.8 (C, C-26), 169.9 (OCOCH<sub>3</sub>), 144.0 (CH, C-3), 129.7 (CH, C-2), 88.0 (C, C-17), 81.7 (C, C-14), 81.5 (CH, C-22), 79.4 (C, C-20), 65.1 (CH<sub>2</sub>, C-18), 63.9 (CH, C-6), 62.1 (C, C-5), 57.6 (C, C-13), 48.5 (C, C-10), 38.4 (CH, C-25), 37.7 (CH<sub>2</sub>, C-16), 36.9 (CH, C-9), 34.2 (CH, C-8), 33.5 (CH<sub>2</sub>, C-23), 32.9 (CH<sub>2</sub>, C-4), 32.8 (CH<sub>2</sub>, C-15), 29.6 (CH, C-24), 26.3 (CH<sub>2</sub>, C-7), 25.6 (CH<sub>2</sub>, C-12), 22.8 (CH<sub>2</sub>, C-11), 21.1 (CH<sub>3</sub>, OCOCH<sub>3</sub>), 18.4 (CH<sub>3</sub>, C-21), 18.2 (CH<sub>3</sub>, C-28), 14.6 (CH<sub>3</sub>, C-19), 12.0 (CH<sub>3</sub>, C-27); HRMS (ESI<sup>+</sup>): calcd for  $C_{30}H_{46}NO_9$  [M + NH<sub>4</sub>]<sup>+</sup> 564.3173, found 564.3157.

(24S,25S)-24,25-dihydrophysachenolide C [(20S,22R,24S,25S)-18acetoxy-24,25-dihydro-5 $\beta$ ,6 $\beta$ -epoxy-14 $\alpha$ ,17 $\beta$ ,20-trihydroxy-1-oxowitha-2-enolide] (12, 1.2 mg, 29%,  $R_f = 0.52$ ) as white amorphous solids: <sup>1</sup>H NMR (400 MHz, CDCl<sub>3</sub>):  $\delta$  6.81 (1H, ddd, J = 10.0, 6.5, 2.3 Hz, H-3), 6.01 (1H, dd, J = 10.0, 2.8 Hz, H-2), 5.08 (1H, dd, J = 12.5, 4.5 Hz, H-22), 4.47 (1H, d, J = 11.5 Hz, Ha-18), 4.26 (1H, d, J = 11.5 Hz, Hb-18), 3.16 (1H, brt, *J* = 1.7 Hz, H-6), 2.93 (1H, dt, *J* = 18.6, 2.6 Hz, Ha-4), 2.64 (1H, m, Ha-16), 2.56 (1H, dq, J = 4.6, 7.1 Hz, H-25), 2.29 (1H, dd, *J* = 12.9, 4.9 Hz, Ha-12), 2.18 (1H, dq, *J* = 4.1, 7.1 Hz, H-24), 2.11 (2H, m, Ha-11, Ha-23), 2.06 (3H, s, OAc), 2.02–1.98 (2H, m, H<sub>2</sub>-7), 1.94 (1H, m, Hb-23), 1.91 (1H, m, H-9), 1.87 (1H, m, H-8), 1.84 (1H, m, Hb-4), 1.77 (1H, brd, J = 12.9 Hz, Hb-12), 1.65 (1H, m, Ha-15), 1.55 (2H, m, Hb-15, Hb-16), 1.42 (1H, m, Hb-11), 1.32 (3H, s, H<sub>3</sub>-21), 1.22 (3H, s,  $H_3$ -19), 1.20 (3H, d, J = 7.1 Hz,  $H_3$ -27), 1.03 (3H, d, J = 7.1Hz, H<sub>3</sub>-28);  ${}^{13}$ C NMR (100 MHz, CDCl<sub>3</sub>):  $\delta$  203.0 (C, C-1), 173.4 (C, C-26), 169.9 (OCOCH<sub>3</sub>), 143.9 (CH, C-3), 129.9 (CH, C-2), 87.9 (C, C-17), 81.5 (C, C-14), 80.8 (CH, C-22), 80.0 (C, C-20), 65.1 (CH $_2$ , C-18), 63.8 (CH, C-6), 62.0 (C, C-5), 57.6 (C, C-13), 48.6 (C, C-10), 40.9 (CH, C-25), 37.5 (CH $_2$ , C-16), 36.9 (CH, C-9), 34.2 (CH, C-8), 33.5 (CH $_2$ , C-23), 32.9 (CH $_2$ , C-4), 32.8 (CH $_2$ , C-15), 30.6 (CH, C-24), 26.2 (CH $_2$ , C-7), 25.5 (CH $_2$ , C-12), 22.7 (CH $_2$ , C-11), 21.1 (CH $_3$ , OCOCH $_3$ ), 18.4 (CH $_3$ , C-21), 14.5 (CH $_3$ , C-19), 14.1 (CH $_3$ , C-28), 13.7 (CH $_3$ , C-27); HRMS (ESI $^+$ ): calcd for C $_3$ 0H $_4$ 6NO $_9$  [M + NH $_4$ ] $^+$ 564.3173, found 564.3170.

 $4\beta$ -Hydroxyphysachenolide D (**20**). A solution of physachenolide D (2, 100.0 mg, 189.4  $\mu$ mol) and SeO<sub>2</sub> (72.9 mg, 662.8  $\mu$ mol) in anhydrous CH<sub>2</sub>Cl<sub>2</sub> (20 mL) was stirred at 25 °C under N<sub>2</sub> for 24 h. To this solution was added SeO<sub>2</sub> (20.8 mg, 189.4  $\mu$ mol), and the solution was refluxed at 45  $^{\circ}\text{C}$  for 30 h. The reaction mixture was then filtered, the filtrate was washed with 2 N HCl (5 mL) and brine (3 × 10 mL), dried over anhydrous Na2SO4, and evaporated under reduced pressure to give a crude product mixture (151.0 mg). This was chromatographed over a column of silica gel (10.0 g) made up in CH<sub>2</sub>Cl<sub>2</sub> and eluted with CH<sub>2</sub>Cl<sub>2</sub> containing increasing amounts of MeOH. Fractions eluted with CH<sub>2</sub>Cl<sub>2</sub>-MeOH (96:4) were combined (45.3 mg) and purified by RP-HPLC using CH<sub>3</sub>CN-H<sub>2</sub>O (35:65) as eluant to give  $4\beta$ hydroxyphysachenolide D [(20S,22R)-18-acetoxy-4 $\beta$ ,14 $\alpha$ ,17 $\beta$ ,20-tetrahydroxy-1-oxowitha-2,5,24-trienolide (20, 40.2 mg, 39%,  $R_t = 18.5$ min) as an amorphous solid;  ${}^{1}H$  NMR (400 MHz, CDCl<sub>3</sub>):  $\delta$  6.76 (1H, dd, J = 10.3, 4.8 Hz, H-3), 5.92 (1H, d, J = 10.3 Hz, H-2), 5.91 (1H, m, H-6), 4.91 (1H, t, J = 7.8 Hz, H-22), 4.61 (1H, d, J = 4.8 Hz, H-4), 4.47 (1H, d, *J* = 11.4, Ha-18), 4.36 (1H, d, *J* = 11.4, Hb-18), 2.70 (1H, m, Ha-16), 2.52 (2H, d, J = 7.8 Hz,  $\text{H}_2$ -23), 2.40 (1H, m, Ha-12), 2.32 (1H, m, Ha-7), 2.30 (1H, m, H-9), 2.26 (1H, m, Ha-11), 2.08 (3H, s, OCOCH<sub>3</sub>), 1.94 (1H, m, Hb-7), 1.93 (3H, s, H<sub>3</sub>-28), 1.88 (3H, s, H<sub>3</sub>-27), 1.82 (1H, s, H-8), 1.76 (1H, m, Hb-12), 1.65 – 1.59 (2H, m, H<sub>2</sub>-15), 1.52 (1H, m, Hb-16), 1.46 (1H, m, Hb-11), 1.42 (3H, s, H<sub>3</sub>-21), 1.41(3H, s, H<sub>3</sub>-19);  ${}^{13}$ C NMR (100 MHz, CDCl<sub>3</sub>):  $\delta$  203.1 (C, C-1), 170.8 (C, COCH<sub>3</sub>), 165.6 (C, C-26), 149.7 (C, C-24), 142.9 (CH, C-3), 138.3 (C, C-5), 131.4 (CH, C-6), 129.4 (CH, C-2), 121.9 (C, C-25), 88.2 (C, C-17), 81.2 (C, C-14), 79.5 (CH, C-22), 78.9 (C, C-20), 69.5 (CH, C-4), 65.2 (CH<sub>2</sub>, C-18), 57.5 (C, C-13), 49.4 (C, C-10), 38.1 (CH<sub>2</sub>, C-16), 37.1 (CH, C-8), 35.8 (CH, C-9), 33.9 (CH<sub>2</sub>, C-23), 33.1 (CH<sub>2</sub>, C-15), 25.9 (CH<sub>2</sub>, C-12), 22.6 (CH<sub>3</sub>, C-19), 22.4 (CH<sub>2</sub>, C-11), 21.3 (CH<sub>3</sub>, CO<u>C</u>H<sub>3</sub>), 20.7 (CH<sub>3</sub>, C-28), 19.2 (CH<sub>3</sub>, C-21), 12.5  $(CH_3, C-27)$ ; HRESIMS 567.2563  $[M + Na]^+$  (calcd for  $C_{30}H_{40}NaO_{9}$ 567.2570).

 $4\beta$ -Hydroxyphysachenolide C (21). To a solution of 20 (32 mg, 58.8  $\mu$ mol) in CH<sub>2</sub>Cl<sub>2</sub> (1.5 mL) at 0 °C was added m-CPBA 77% (20 mg, 89.2  $\mu$ mol), and the mixture was stirred at 0 °C for 5 min. The ice bath was removed, and the reaction mixture was stirred at 25 °C (TLC controlled). After 4 h, the reaction mixture was concentrated and chromatographed over a column of silica gel (2.0 g) made up in CH<sub>2</sub>Cl<sub>2</sub> and eluted with CH<sub>2</sub>Cl<sub>2</sub> containing increasing amounts of MeOH. Fractions eluted with CH<sub>2</sub>Cl<sub>2</sub>-MeOH (96:4) were combined to give  $4\beta$ -hydroxyphysachenolide C [(20S,22R)-18-acetoxy- $5\beta$ , $6\beta$ -epoxy- $4\beta$ ,  $14\alpha$ ,  $17\beta$ , 20-tetrahydroxy-1-oxowitha-2, 24-dienolide (21, 20.3 mg, 62%) as an amorphous solid; <sup>1</sup>H NMR (400 MHz, CDCl<sub>3</sub>):  $\delta$  6.90 (1H, dd, J = 9.9, 5.9 Hz, H-3), 6.18 (1H, d, J = 9.9 Hz, H-2), 4.85 (1H, dd, J =10.1, 7.1 Hz, H-22), 4.37 (1H, d, J = 11.7, Ha-18), 4.27 (1H, d, J = 11.7, Hb-18), 3.71 (1H, dd, *J* = 5.9, 2.1 Hz, H-4), 3.25 (1H, brs, H-6), 2.65 (1H, m, Ha-16), 2.50 (2H, m,  $H_2$ -23), 2.20 (1H, dt, J = 12.7, 4.4 Hz, Ha-12), 2.07 (3H, s, OCOC $H_3$ ), 2.00 (2H, m,  $H_2-7$ ), 1.93 (3H, s,  $H_3-7$ ) 28), 1.88 (3H, s, H<sub>3</sub>-27), 1.77 (1H, m, Ha-11), 1.76 (1H, m, H-9), 1.73 (1H, m, Hb-12), 1.72 (1H, m, H-8), 1.64–1.56 (2H, m, H<sub>2</sub>-15), 1.53 (1H, m, Hb-16), 1.35 (1H, m, Hb-11), 1.39 (3H, s, H<sub>3</sub>-21), 1.38 (3H, s,  $H_3$ -19); <sup>13</sup>C NMR (100 MHz, CDCl<sub>3</sub>): δ 201.7 (C, C-1), 170.0 (C, COCH<sub>3</sub>), 165.6 (C, C-26), 149.7 (C, C-24), 141.5(CH, C-3), 132.8 (CH, C-2), 121.9 (C, C-25), 87.9 (C, C-17), 81.3 (C, C-14), 79.4 (CH, C-22), 78.9 (C, C-20), 70.1 (CH, C-4), 64.8 (CH<sub>2</sub>, C-18), 63.9 (C, C-5), 62.8 (CH, C-6), 57.4 (C, C-13), 47.6 (C, C-10), 38.1 (CH<sub>2</sub>, C-16), 36.6 (CH, C-8), 34.2 (CH, C-9), 33.9 (CH<sub>2</sub>, C-23), 32.9 (CH<sub>2</sub>, C-15), 25.9 (CH<sub>2</sub>, C-7), 25.3 (CH<sub>2</sub>, C-12), 21.5 (CH<sub>2</sub>, C-11), 21.3 (CH<sub>3</sub>, COCH<sub>3</sub>), 20.6 (CH<sub>3</sub>, C-28), 19.1 (CH<sub>3</sub>, C-19), 16.8 (CH<sub>3</sub>, C-20), 12.4  $(CH_3, C-27)$ ; HRESIMS 578.2951  $[M + NH_4]^+$  (calcd for  $C_{30}H_{44}NO_{10}$ 578.2965).

 $4\beta$ -O-Fmoc-Glycylphysachenolide C (22). To a solution of 21 (10.0 mg, 17.8  $\mu \mathrm{mol})$  in anhydrous EtOAc (2.0 mL) was added Fmoc-glycine (12.8 mg, 43.0  $\mu$ mol), DCC (10.0 mg, 48.5  $\mu$ mol), and 4-pp (ca 1.0 mg) and stirred at 25 °C for 90 min (TLC control). The reaction mixture was filtered, the filtrate was evaporated under reduced pressure, and the residue was chromatographed over a column of silica gel (1.0 g) made up in EtOAc-hexanes (60:40) and eluted with EtOAc-hexanes (60:40) followed by EtOAc-hexanes (70:30). Fractions eluted with EtOAc-hexanes (70:30) were combined to give  $4\beta$ -O-Fmocglycylphysachenolide C [(20S,22R)-18-acetoxy-5 $\beta$ ,6 $\beta$ -epoxy-4 $\beta$ -O-Fmoc-glycyl- $4\alpha$ ,  $17\beta$ , 20-trihydroxy-1-oxowitha-2, 24-dienolide (22, 13.3 mg, 89%) as an amorphous solid; <sup>1</sup>H NMR (400 MHz, CDCl<sub>3</sub>):  $\delta$  7.73 (2H, d, J = 7.7 Hz, H-11', H-12'), 7.57 (2H, brd, J = 7.7 Hz, H-8', H-15'), 7.38 (2H, d, t = 7.7 Hz, H-10', H-13'), 7.29 (2H, td, J = 7.7, 1.2 Hz, H-9', H-14'), 6.97 (1H, dd, *J* = 10.1, 6.5 Hz, H-3), 6.25 (1H, d, *J* = 10.1 Hz, H-2), 5.23 (1H, t, *J* = 5.8 Hz, NH), 4.82 (1H, dd, *J* = 12.4, 6.6 Hz, H-22), 4.40 (1H, d, J = 11.7, Ha-18), 4.36 (2H, m, H<sub>2</sub>-6'), 4.22 (1H, d, J = 11.7, Hb-18), 4.72 (1H, d, J = 6.5 Hz, H-4), 3.96 (2H, m, H<sub>2</sub>-2'), 3.45 (1H, m, H-7'), 3.26 (1H, brs, H-6), 2.66 (1H, m, Ha-16), 2.50 (2H, m, H<sub>2</sub>-23), 2.16 (1H, m, Ha-12), 2.07 (3H, s, OAc), 2.05 (2H, m, H<sub>2</sub>-7), 1.91 (3H, s, H<sub>3</sub>-28), 1.89 (1H, m, Ha-11), 1.87 (3H, s, H<sub>3</sub>-27), 1.75 (1H, m, H-9), 1.70 (1H, m, Hb-12), 1.64 (4H, m, H-8, Hb-12, H<sub>2</sub>-15), 1.38 (3H, s, H<sub>3</sub>-21), 1.35 (3H, s, H<sub>3</sub>-19); <sup>13</sup>C NMR (100 MHz, CDCl<sub>3</sub>): δ 200.4 (C, C-1), 170.0 (C, OAc), 169.2 (C, C-1'), 165.6 (C, C-26), 156.1 (C, C-4'), 149.8 (C, C-24), 143.7 (C, C-7'a, C-15'a), 141.2 (C, C11'a, C-11'b), 138.5 (CH, C-3), 134.7 (C, C-2), 127.7 (CH, C-10', C-13'), 127.0 (CH, C-9', C-14'), 125.1 (CH, C-8', C-15'), 121.8 (C, C-25), 119.9 (CH, C-11', C-12'), 87.8 (C, C-17), 81.1 (C, C-14), 79.4 (CH, C-22), 78.8 (C, C-20), 73.2 (CH, C-4), 67.3 (CH<sub>2</sub>, C-6'), 64.7 (CH<sub>2</sub>, C-18), 61.1 (C, C-5), 60.9 (CH, C-6), 57.4 (C, C-13), 49.2 (CH, C-7'), 47.9 (C, C-10), 42.6 (CH<sub>2</sub>, C-2'), 38.0 (CH<sub>2</sub>, C-16), 36.7 (CH, C-8), 34.0 (CH<sub>2</sub>, C-23), 33.9 (CH, C-9), 32.8 (CH<sub>2</sub>, C-15), 25.6 (CH<sub>2</sub>, C-7), 24.9 (CH<sub>2</sub>, C-12), 21.3 (CH<sub>3</sub>, OAc), 21.0 (CH<sub>2</sub>, C-11), 20.6 (CH<sub>3</sub>, C-28), 19.0 (CH<sub>3</sub>, C-21), 15.3 (CH<sub>3</sub>, C-19), 12.4 (CH<sub>3</sub>, C-27).

 $4\beta$ -O-Glycylphysachenolide C (23). To a solution of 22 (13.0 mg, 15.4  $\mu$ mol) in anhydrous THF (2.0 mL) at 0 °C was added 1 M TBAF in THF (20  $\mu$ L) and stirred at 0 °C for 5 h (TLC control). The reaction mixture was diluted with EtOAc (15.0 mL), washed with brine ( $3 \times 5.0$ mL), and evaporated under reduced pressure, and the residue was chromatographed over a column of silica gel (0.5 g) made up in CH<sub>2</sub>Cl<sub>2</sub> and eluted with CH<sub>2</sub>Cl<sub>2</sub>, CH<sub>2</sub>Cl<sub>2</sub>-MeOH (96:4), and CH<sub>2</sub>Cl<sub>2</sub>-MeOH (92:8). Fractions eluted with CH<sub>2</sub>Cl<sub>2</sub>-MeOH (92:8) were combined to give  $4\beta$ -O-glycylphysachenolide C [(20S,22R)-18-acetoxy-5 $\beta$ ,6 $\beta$ epoxy- $4\beta$ -O-glycyl- $4\alpha$ ,17 $\beta$ ,20-trihydroxy-1-oxowitha-2,24-dienolide] (23, 9.0 mg, 94.0%) as an amorphous solid; <sup>1</sup>H NMR (400 MHz, CDCl<sub>3</sub>):  $\delta$  6.99 (1H, dd, J = 10.2, 6.5 Hz, H-3), 6.23 (1H, d, J = 10.2Hz), 4.82 (1H, dd, J = 10.9, 7.0 Hz, H-22), 4.69 (1H, d, J = 6.5 Hz, H-4), 4.37 (1H, d, J = 11.9 Hz, Ha-18), 4.23 (1H, d. J = Hb-18), 3.45 (1H, d, J = 18.3 Hz, Ha-2), 3.35 (1H, d, J = 18.3 Hz, Hb-2), 3.26 (1H, brs, H-6), 2.65 (1H, m, Ha-16), 2.50 (2H, m, H<sub>2</sub>-23), 2.21 (1H, m, Ha-12), 2.07 (3H, s, OAc), 1.91 (3H, s, H<sub>3</sub>-28), 1.87 (3H, s, H<sub>3</sub>-27), 1.38 (3H, s, H<sub>3</sub>-21), 1.34 (3H, s, H<sub>3</sub>-19).

14: To a solution of 23 (8.0 mg, 12.9  $\mu$ mol) in anhydrous DMF (1.0 mL) was added NHS-fluorescein (6.7 mg, 14.2  $\mu$ mol) and DIPEA (18.0  $\mu$ L) and stirred at 25 °C for 4 h (TLC control). Solvent was evaporated under reduced pressure and by adding n-heptane, the residue was chromatographed over a column of silica gel (0.5 g) using CH<sub>2</sub>Cl<sub>2</sub>-MeOH (92:8) as eluant, and the product was further purified by RP-TLC using MeOH-H<sub>2</sub>O (70:30) to give 14 (9.1 mg, 73%) as an amorphous solid (mixture of 2 isomers with the ratio of 1:0.7); <sup>1</sup>H NMR (400 MHz, CDCl<sub>3</sub>+ CD<sub>3</sub>OD) (of major isomer):  $\delta$  8.31 (1H, d, J = 2.0 Hz, ArH), 8.14 (1H, dd, J = 8.0, 2.0 Hz, ArH), 7.98 (2H, m, ArH),7.80 (1H, t, J = 5.4 Hz, NH), 7.19 (1H, d, J = 8.0 Hz, ArH), 6.96 (1H, dd, J = 9.8, 6.0 Hz, H-3),  $6.62 (2\text{H}, \text{m}, 2 \times \text{ArH}), 6.50-6.40 (3\text{H}, \text{m}, 3 \times \text{Hz})$ ArH), 6.19 (1H, d, J = 9.8 Hz, H-2), 4.70 (1H, dd, J = 13.2, 3.2 Hz, H-22), 4.70 (1H, d, J = 6.0 Hz, H-4), 4.32 (1H, d, J = 11.9 Hz, Ha-18), 4.15  $(1H, d, J = 6.0 \text{ Hz}, \text{Ha-COC}H_2\text{NH}), 4.06 (1H, d, J = 11.9 \text{ Hz}, \text{Hb-}18),$  $4.03 (1H, d, J = 6.0 \text{ Hz}, \text{Hb-COC}H_2\text{NH}), 3.25 (1H, \text{brt}, J = 2.0 \text{ H}, \text{H-6}),$ 2.58 (1H, m, Ha-16), 2.56 (2H H, m, H<sub>2</sub>-23), 2.11 (1H, m, Ha-12),

2.01 (3H, s, OAc), 1.97–1.93 (2H, m, H<sub>2</sub>-7), 1.87 (3H, s, H<sub>3</sub>-28), 1.82 (1H, m, Ha-11), 1.79 (3H, s, H<sub>3</sub>-27), 1.70 (1H, m, Hb-12), 1.68 (1H, m, H-9), 1.60-1.54 (3H, m, H-8, Hb-11, Ha-15), 1.48 (2H, m, Hb-15, Hb-16), 1.27 (3H, s, H<sub>3</sub>-21), 1.25 (3H, s, H<sub>3</sub>-19); <sup>13</sup>C NMR (100 MHz, CDCl<sub>3</sub> + CD<sub>3</sub>OD) (of major isomer):  $\delta$  200.8 (C, C-1), 171.0 (C, OAc), 169.3 (C, OCOCH<sub>2</sub>), 169.0 (C, CONH), 167.4 (C, CO<sub>2</sub>H), 166.3 (C, C-26), 159.4 (C, ArC-OH), 152.6 (C, ArC-O), 152.5 (C, ArC-O), 151.1 (C, C-24), 138.7 (CH, C-3), 134.5 (CH, C-2), 129.0 (CH, ArC), 124.7 (CH, ArC), 123.5 (CH, ArC), 121.2 (C, ArC). 112.4 (CH, ArC), 87.5 (C, C-13), 81.0 (CH, C-22), 80.7 (C, C-14), 78.2 (C, C-20), 73.2 (CH, C-4), 64.6 (CH<sub>2</sub>, C-18), 61.2 (CH, C-6), 60.9 (C, C-5), 57.1 (C, C-13), 47.9 (C, C-10), 41.6 (CH<sub>2</sub>, COCH<sub>2</sub>NH), 37.5 (CH<sub>2</sub>, C-16), 36.7 (CH, C-8), 33.0 (CH, C-9), 33.9 (CH, C-9), 33.7 (CH<sub>2</sub>, C-22), 32.6 (CH<sub>2</sub>, C-15), 25.6 (CH<sub>2</sub>, C-7), 24.8 (CH<sub>2</sub>, C-12), 21.2 (CH<sub>3</sub>, OAc), 20.9 (CH<sub>2</sub>, C-11), 20.5 (CH<sub>3</sub>, C-28), 18.2 (CH<sub>3</sub>, C-21), 15.2 (CH<sub>3</sub>, C-19), 12.1 (CH<sub>3</sub>, C-27); <sup>1</sup>H NMR (400 MHz,  $CDCl_3 + CD_3OD$ ) (of minor isomer):  $\delta$  8.12 (1H, m, ArH), 7.50 (1H, s, ArH), 7.1 (1H, d, J = 8.0 Hz, ArH), 6.89 (1H, dd, J = 9.8, 6.0 Hz, H-3), 6.61 (2H, m,  $2 \times ArH$ ), 6.50–6.40 (4H, m,  $4 \times ArH$ ), 6.14 (1H, d, J =9.8 Hz, H-2), 4.70 (1H, dd, *J* = 13.2, 3.2 Hz, H-22), 4.62 (1H, d, *J* = 6.0 Hz, H-4), 4.32 (1H, d, J = 11.9 Hz, Ha-18), 4.15 (1H, d, J = 6.0 Hz, Ha- $COCH_2NH$ ), 4.06 (1H, d, J = 11.9 Hz, Hb-18), 4.03 (1H, d, J = 6.0 Hz, Hb-COC $H_2$ NH), 4.01 (0.7H, d, J = 6.0 Hz, Hb-COC $H_2$ NH), 3.21 (H, brt, J = 2.0 H, H-6), 2.58 (1H, m, Ha-16), 2.40 (2 H, m, H<sub>2</sub>-23), 2.11 (1H, m, Ha-12), 2.02 (3 H, s, OAc), 1.97-1.93 (2H, m, H<sub>2</sub>-7), 1.87 (3H, s, H<sub>3</sub>-28), 1.82 (1H, m, Ha-11), 1.79 (3H, s, H<sub>3</sub>-27), 1.70 (1H, m, Hb-12), 1.68 (1 Hz, m, H-9), 1.60–1.54 (3H, m, H-8, Hb-11, Ha-15), 1.48 (2H, m, Hb-15, Hb-16), 1.27 (3H, s, H<sub>3</sub>-21), 1.25 (3H, s, H<sub>3</sub>-19), 1.17 (3H, s, H<sub>3</sub>-19); <sup>13</sup>C NMR of minor isomer (100 MHz, CDCl<sub>3</sub> + CD<sub>3</sub>OD) (of minor isomer):  $\delta$  200.7 (C, C-1), 171.2 (C, OAc), 169.1 (C, OCOCH<sub>2</sub>), 168.8 (C, CONH), 167.4 (C, CO<sub>2</sub>H), 166.2 (C, C-26), 159.4 (C, ArC-OH), 152.6 (C, ArC-O), 152.5 (C, ArC-O), 151.1 (C, C-24), 138.6 (CH, C-3), 135.4 (C, arC), 134.7 (CH, C-2), 128.9 (CH, ArC), 127.2 (C, ArC), 125.3 (CH, ArC), 122.7 (CH, ArC), 112.4 (CH, ArC), 109.5 (C, ArC), 102.7 (CH, ArC), 87.4 (C, C-13), 80.9 (CH, C-22), 80.7 (C, C-14), 78.2 (C, C-20), 73.2 (CH, C-4), 64.7 (CH<sub>2</sub>, C-18), 61.3 (CH, C-6), 60.8 (C, C-5), 57.0 (C, C-13), 47.8 (C, C-10), 41.5 (CH<sub>2</sub>, COCH<sub>2</sub>NH), 37.5 (CH<sub>2</sub>, C-16), 36.6 (CH, C-8), 33.8 (CH, C-9), 33.7 (CH<sub>2</sub>, C-22), 32.6 (CH<sub>2</sub>, C-15), 25.5 (CH<sub>2</sub>, C-7), 24.8 (CH<sub>2</sub>, C-12), 21.3 (CH<sub>3</sub>, OAc), 20.9 (CH<sub>2</sub>, C-11), 20.5 (CH<sub>3</sub>, C-28), 18.1 (CH<sub>3</sub>, C-21), 15.1 (CH<sub>3</sub>, C-19), 12.1 (CH<sub>3</sub>, C-27); HRESIMS 998.3198 [M + Na]<sup>+</sup> (calcd for C<sub>53</sub>H<sub>53</sub>NNaO<sub>17</sub> 998.3211).

## ASSOCIATED CONTENT

#### Supporting Information

The Supporting Information is available free of charge at https://pubs.acs.org/doi/10.1021/acs.jmedchem.2c01770.

Bromodomain protein used for all biochemical and structural studies; X-ray crystallography data collection and refinement statistics; comparison of PCC and (+)-JQ1 binding to BRD3-BD1; BRD2 and BRDT FP assay data; identification of cellular Biotin-PCC interactors by LC-MS/MS; <sup>1</sup>H NMR spectra of 10–12 and 14–23; <sup>13</sup>C NMR spectra of 10–12, 14–17, and 20–22; <sup>1</sup>H–<sup>1</sup>H COSY spectra of 10–12, 16, and 20; HSQC spectra of 10–12, 14–17, and 20–22; HMBC spectra of 10, 11, 15, 17, and 20; <sup>1</sup>H and 1D NOESY spectra of 11 and 12; HPLC chromatograms of PCC and 10–12 (PDF)

Molecular formula strings for all assayed compounds (CSV)

#### **Accession Codes**

Protein Data Bank (PDB): The models and structure factors have been deposited under accession codes: 7R8R (BRD3-BD1 + PCC) and 7S3P (BRD3-BD2 + PCC). Biomagnetic Resonance Bank (BMRB): the chemical shifts and atomic

assignments have been deposited under accession codes: 50801 (BRD3-BD1) and 50802 (BRD3-BD1 + PCC). Authors will release the atomic coordinates and experimental data upon article publication. New Address for Andrew J. Ambrose: Small Molecule Discovery Center, Department of Pharmaceutical Chemistry and Helen Diller Family Comprehensive Cancer Center, University of California, San Francisco, 1700 4th Street, San Francisco, California 94143, United States

#### AUTHOR INFORMATION

## **Corresponding Authors**

A. A. Leslie Gunatilaka — College of Agriculture and Life Sciences, School of Natural Resources and the Environment, Southwest Center for Natural Products Research, University of Arizona, Tucson, Arizona 85706, United States; Email: LeslieG@cals.arizona.edu

Raimund Fromme — School of Molecular Sciences, Biodesign Institute, Arizona State University, Tempe, Arizona 85287, United States; Email: Raimund.Fromme@asu.edu

Eli Chapman — College of Pharmacy, Department of Pharmacology and Toxicology, University of Arizona, Tucson, Arizona 85721, United States; oorcid.org/0000-0002-6310-1664; Email: chapman@pharmacy.arizona.edu

### **Authors**

Christopher J. Zerio — College of Pharmacy, Department of Pharmacology and Toxicology, University of Arizona, Tucson, Arizona 85721, United States; Present Address: Present address: Department of Integrative Structural and Computational Biology, Scripps Research, Hazen 175, 10,630 John J. Hopkins Drive, La Jolla, California 92121, United States (C.J.Z.); orcid.org/0000-0003-4053-4835

Jared Sivinski — College of Pharmacy, Department of Pharmacology and Toxicology, University of Arizona, Tucson, Arizona 85721, United States

E. M. Kithsiri Wijeratne — College of Agriculture and Life Sciences, School of Natural Resources and the Environment, Southwest Center for Natural Products Research, University of Arizona, Tucson, Arizona 85706, United States

Ya-Ming Xu — College of Agriculture and Life Sciences, School of Natural Resources and the Environment, Southwest Center for Natural Products Research, University of Arizona, Tucson, Arizona 85706, United States

Duc T. Ngo – College of Pharmacy, Department of Pharmacology and Toxicology, University of Arizona, Tucson, Arizona 85721, United States

Andrew J. Ambrose — College of Pharmacy, Department of Pharmacology and Toxicology, University of Arizona, Tucson, Arizona 85721, United States; Present Address: Present address: Small Molecule Discovery Center, Department of Pharmaceutical Chemistry and Helen Diller Family Comprehensive Cancer Center, University of California, San Francisco, 1700 4th Street, San Francisco, California 94143, United States (A.J.A.); orcid.org/0000-0002-2932-4514

Luis Villa-Celis — College of Pharmacy, Department of Pharmacology and Toxicology, University of Arizona, Tucson, Arizona 85721, United States

Niloofar Ghadirian — Department of Molecular and Cellular Biology, University of Arizona, Tucson, Arizona 85721, United States Michael W. Clarkson – Department of Chemistry and Biochemistry, University of Arizona, Tucson, Arizona 85719, United States

Donna D. Zhang — College of Pharmacy, Department of Pharmacology and Toxicology, University of Arizona, Tucson, Arizona 85721, United States

Nancy C. Horton — Department of Molecular and Cellular Biology, University of Arizona, Tucson, Arizona 85721, United States

Complete contact information is available at: https://pubs.acs.org/10.1021/acs.jmedchem.2c01770

#### **Author Contributions**

<sup>†</sup>C.J.Z. and J.S. contributed equally to this work.

#### Notes

The authors declare the following competing financial interest(s): Eli Chapman is a cofounder of BioEL, Inc.

### ACKNOWLEDGMENTS

C.J.Z., J.S., and A.J.A. are funded by T32 GM008804. DDZ is supported by National Institutes of Health grant R35ES031575. This work was supported in part by a grant from the Arizona Biomedical Research Center (grant number ADHS-16-162515). 22Rv1 cells were kindly provided by Dr. Len Neckers (NCI, Bethesda, MD, USA). We would like to acknowledge Dr. May Khanna for graciously allowing us to use her AlphaScreen assay reader. We would also like to thank Ms. Manping X. Liu for some cytotoxicity assay data and Dr. Qin M. Chen for graciously allowing us to use her Microscale Thermophoresis instrument.

### ABBREVIATIONS

ADT, androgen deprivation therapy; Alpha, amplified luminescent proximity homogenous assay; AR, androgen receptor; BD, bromodomain; BET, bromodomain and extra-terminal; Bt-PCC, biotinylated PCC; CHX, cycloheximide; CRPC, castration-resistant prostate cancer; CSP, chemical shift perturbation; DSF, differential scanning fluorimetry; DUB, deubiquitinase; FP, fluorescence polarization; HSQC, heteronuclear single quantum coherence;  $K_{\rm ac}$ , N-acetyl lysine; MST, microscale thermophoresis; PC, prostate cancer; PCC, physachenolide C; PROTAC, proteolysis-targeting chimera; PSA, prostate-specific antigen; qRT-PCR, quantitative reverse transcription polymerase chain reaction; SAR, structure—activity relationships;  $T_{\rm m}$ , melting temperature; TSA, thermal shift assay; UPP, ubiquitin proteasome pathway; 17-BHW,  $17\beta$ -hydroxywithanolide.

## REFERENCES

- (1) Centers for Disease Control and Prevention. *Prostate Cancer Statistics*.; Centers for Disease Control and Prevention: https://www.cdc.gov/cancer/prostate/statistics/index.htm (accessed 2021-04-07).
- (2) Key Statistics for Prostate Cancer | Prostate Cancer Facts.; American Cancer Society https://www.cancer.org/cancer/prostate-cancer/about/key-statistics.html (accessed 2021-04-07).
- (3) Teply, B. A.; Antonarakis, E. S. Novel Mechanism-Based Therapeutics for Androgen Axis Blockade in Castration-Resistant Prostate Cancer. *Curr. Opin. Endocrinol. Diabetes Obes.* **2016**, 23, 279–290
- (4) Bluemn, E. G.; Coleman, I. M.; Lucas, J. M.; Coleman, R. T.; Hernandez-Lopez, S.; Tharakan, R.; Bianchi-Frias, D.; Dumpit, R. F.; Kaipainen, A.; Corella, A. N.; Yang, Y. C.; Nyquist, M. D.; Mostaghel, E.; Hsieh, A. C.; Zhang, X.; Corey, E.; Brown, L. G.; Nguyen, H. M.; Pienta, K.; Ittmann, M.; Schweizer, M.; True, L. D.; Wise, D.; Rennie, P.

- S.; Vessella, R. L.; Morrissey, C.; Nelson, P. S. Androgen Receptor Pathway-Independent Prostate Cancer Is Sustained through FGF Signaling. *Cancer Cell* **2017**, *32*, 474–489.e6.
- (5) Ciccarese, C.; Santoni, M.; Brunelli, M.; Buti, S.; Modena, A.; Nabissi, M.; Artibani, W.; Martignoni, G.; Montironi, R.; Tortora, G.; Massari, F. AR-V7 and Prostate Cancer: The Watershed for Treatment Selection? *Cancer Treat. Rev.* **2016**, *43*, 27–35.
- (6) Visakorpi, T.; Hyytinen, E.; Koivisto, P.; Tanner, M.; Keinänen, R.; Palmberg, C.; Palotie, A.; Tammela, T.; Isola, J.; Kallioniemi, O. P. In Vivo Amplification of the Androgen Receptor Gene and Progression of Human Prostate Cancer. *Nat. Genet.* 1995, *9*, 401–406.
- (7) Urbanucci, A.; Mills, I. G. Bromodomain-Containing Proteins in Prostate Cancer. *Mol. Cell. Endocrinol.* **2018**, *462*, 31–40.
- (8) Roudier, M. P.; True, L. D.; Higano, C. S.; Vesselle, H.; Ellis, W.; Lange, P.; Vessella, R. L. Phenotypic Heterogeneity of End-Stage Prostate Carcinoma Metastatic to Bone. *Hum. Pathol.* **2003**, *34*, 646–653.
- (9) Shah, R. B.; Mehra, R.; Chinnaiyan, A. M.; Shen, R.; Ghosh, D.; Zhou, M.; Macvicar, G. R.; Varambally, S.; Harwood, J.; Bismar, T. A.; Kim, R.; Rubin, M. A.; Pienta, K. J. Androgen-Independent Prostate Cancer Is a Heterogeneous Group of Diseases: Lessons from a Rapid Autopsy Program. *Cancer Res.* **2004**, *64*, 9209–9216.
- (10) Culig, Z.; Santer, F. R. Androgen Receptor Signaling in Prostate Cancer. *Cancer Metastasis Rev.* **2014**, *33*, 413–427.
- (11) Rohira, A. D.; Lonard, D. M. Steroid Receptor Coactivators Present a Unique Opportunity for Drug Development in Hormone-Dependent Cancers. *Biochem. Pharmacol.* **2017**, *140*, 1–7.
- (12) Meslamani, J.; Smith, S. G.; Sanchez, R.; Zhou, M.-M. Structural Features and Inhibitors of Bromodomains. *Drug Discov. Today Technol.* **2016**, *19*, 3–15.
- (13) Filippakopoulos, P.; Knapp, S. Targeting Bromodomains: Epigenetic Readers of Lysine Acetylation. *Nat. Rev. Drug Discov.* **2014**, *13*, 337–356.
- (14) Filippakopoulos, P.; Picaud, S.; Mangos, M.; Keates, T.; Lambert, J.-P.; Barsyte-Lovejoy, D.; Felletar, I.; Volkmer, R.; Müller, S.; Pawson, T.; Gingras, A.-C.; Arrowsmith, C. H.; Knapp, S. Histone Recognition and Large-Scale Structural Analysis of the Human Bromodomain Family. *Cell* **2012**, *149*, 214–231.
- (15) Nicodeme, E.; Jeffrey, K. L.; Schaefer, U.; Beinke, S.; Dewell, S.; Chung, C.; Chandwani, R.; Marazzi, I.; Wilson, P.; Coste, H.; White, J.; Kirilovsky, J.; Rice, C. M.; Lora, J. M.; Prinjha, R. K.; Lee, K.; Tarakhovsky, A. Suppression of Inflammation by a Synthetic Histone Mimic. *Nature* **2010**, *468*, 1119–1123.
- (16) Dawson, M. A.; Prinjha, R. K.; Dittmann, A.; Giotopoulos, G.; Bantscheff, M.; Chan, W.-I.; Robson, S. C.; Chung, C.; Hopf, C.; Savitski, M. M.; Huthmacher, C.; Gudgin, E.; Lugo, D.; Beinke, S.; Chapman, T. D.; Roberts, E. J.; Soden, P. E.; Auger, K. R.; Mirguet, O.; Doehner, K.; Delwel, R.; Burnett, A. K.; Jeffrey, P.; Drewes, G.; Lee, K.; Huntly, B. J. P.; Kouzarides, T. Inhibition of BET Recruitment to Chromatin as an Effective Treatment for MLL-Fusion Leukaemia. *Nature* 2011, 478, 529–533.
- (17) Delmore, J. E.; Issa, G. C.; Lemieux, M. E.; Rahl, P. B.; Shi, J.; Jacobs, H. M.; Kastritis, E.; Gilpatrick, T.; Paranal, R. M.; Qi, J.; Chesi, M.; Schinzel, A. C.; McKeown, M. R.; Heffernan, T. P.; Vakoc, C. R.; Bergsagel, P. L.; Ghobrial, I. M.; Richardson, P. G.; Young, R. A.; Hahn, W. C.; Anderson, K. C.; Kung, A. L.; Bradner, J. E.; Mitsiades, C. S. BET Bromodomain Inhibition as a Therapeutic Strategy to Target C-Myc. *Cell* 2011, 146, 904–917.
- (18) Zuber, J.; Shi, J.; Wang, E.; Rappaport, A. R.; Herrmann, H.; Sison, E. A.; Magoon, D.; Qi, J.; Blatt, K.; Wunderlich, M.; Taylor, M. J.; Johns, C.; Chicas, A.; Mulloy, J. C.; Kogan, S. C.; Brown, P.; Valent, P.; Bradner, J. E.; Lowe, S. W.; Vakoc, C. R. RNAi Screen Identifies Brd4 as a Therapeutic Target in Acute Myeloid Leukaemia. *Nature* **2011**, 478, 524–528.
- (19) Asangani, I. A.; Dommeti, V. L.; Wang, X.; Malik, R.; Cieslik, M.; Yang, R.; Escara-Wilke, J.; Wilder-Romans, K.; Dhanireddy, S.; Engelke, C.; Iyer, M. K.; Jing, X.; Wu, Y.-M.; Cao, X.; Qin, Z. S.; Wang, S.; Feng, F. Y.; Chinnaiyan, A. M. Therapeutic Targeting of BET Bromodomain

- Proteins in Castration-Resistant Prostate Cancer. Nature 2014, 510, 278-282.
- (20) French, C. A.; Ramirez, C. L.; Kolmakova, J.; Hickman, T. T.; Cameron, M. J.; Thyne, M. E.; Kutok, J. L.; Toretsky, J. A.; Tadavarthy, A. K.; Kees, U. R.; Fletcher, J. A.; Aster, J. C. BRD-NUT Oncoproteins: A Family of Closely Related Nuclear Proteins That Block Epithelial Differentiation and Maintain the Growth of Carcinoma Cells. *Oncogene* 2008, 27, 2237–2242.
- (21) Gaudio, E.; Tarantelli, C.; Ponzoni, M.; Odore, E.; Rezai, K.; Bernasconi, E.; Cascione, L.; Rinaldi, A.; Stathis, A.; Riveiro, E.; Cvitkovic, E.; Zucca, E.; Bertoni, F. Bromodomain Inhibitor OTX015 (MK-8628) Combined with Targeted Agents Shows Strong in Vivo Antitumor Activity in Lymphoma. *Oncotarget* 2016, 7, 58142–58147. (22) Filippakopoulos, P.; Qi, J.; Picaud, S.; Shen, Y.; Smith, W. B.; Fedorov, O.; Morse, E. M.; Keates, T.; Hickman, T. T.; Felletar, I.; Philpott, M.; Munro, S.; McKeown, M. R.; Wang, Y.; Christie, A. L.; West, N.; Cameron, M. J.; Schwartz, B.; Heightman, T. D.; La Thangue, N.; French, C. A.; Wiest, O.; Kung, A. L.; Knapp, S.; Bradner, J. E.
- (23) Asangani, I. A.; Wilder-Romans, K.; Dommeti, V. L.; Krishnamurthy, P. M.; Apel, I. J.; Escara-Wilke, J.; Plymate, S. R.; Navone, N. M.; Wang, S.; Feng, F. Y.; Chinnaiyan, A. M. BET Bromodomain Inhibitors Enhance Efficacy and Disrupt Resistance to AR Antagonists in the Treatment of Prostate Cancer. *Mol. Cancer Res.* **2016**, *14*, 324–331.

Selective Inhibition of BET Bromodomains. Nature 2010, 468, 1067-

- (24) Trabucco, S. E.; Gerstein, R. M.; Evens, A. M.; Bradner, J. E.; Shultz, L. D.; Greiner, D. L.; Zhang, H. Inhibition of Bromodomain Proteins for the Treatment of Human Diffuse Large B-Cell Lymphoma. *Clin. Cancer Res.* **2015**, *21*, 113–122.
- (25) Alqahtani, A.; Choucair, K.; Ashraf, M.; Hammouda, D. M.; Alloghbi, A.; Khan, T.; Senzer, N.; Nemunaitis, J. Bromodomain and Extra-Terminal Motif Inhibitors: A Review of Preclinical and Clinical Advances in Cancer Therapy. *Future Sci. OA* **2019**, *5*, FSO372.
- (26) Li, Z.; Wang, D.; Li, L.; Pan, S.; Na, Z.; Tan, C. Y. J.; Yao, S. Q. "Minimalist" Cyclopropene-Containing Photo-Cross-Linkers Suitable for Live-Cell Imaging and Affinity-Based Protein Labeling. *J. Am. Chem. Soc.* **2014**, *136*, 9990–9998.
- (27) Tsume, M.; Kimura-Yoshida, C.; Mochida, K.; Shibukawa, Y.; Amazaki, S.; Wada, Y.; Hiramatsu, R.; Shimokawa, K.; Matsuo, I. Brd2 Is Required for Cell Cycle Exit and Neuronal Differentiation through the E2F1 Pathway in Mouse Neuroepithelial Cells. *Biochem. Biophys. Res. Commun.* **2012**, 425, 762–768.
- (28) Wang, F.; Liu, H.; Blanton, W. P.; Belkina, A.; Lebrasseur, N. K.; Denis, G. V. Brd2 Disruption in Mice Causes Severe Obesity without Type 2 Diabetes. *Biochem. J.* **2010**, *425*, 71–85.
- (29) Lambert, J.-P.; Picaud, S.; Fujisawa, T.; Hou, H.; Savitsky, P.; Uusküla-Reimand, L.; Gupta, G. D.; Abdouni, H.; Lin, Z.-Y.; Tucholska, M.; Knight, J. D. R.; Gonzalez-Badillo, B.; St-Denis, N.; Newman, J. A.; Stucki, M.; Pelletier, L.; Bandeira, N.; Wilson, M. D.; Filippakopoulos, P.; Gingras, A.-C. Interactome Rewiring Following Pharmacological Targeting of BET Bromodomains. *Mol. Cell* **2019**, 73, 621–638.e17.
- (30) Gamsjaeger, R.; Webb, S. R.; Lamonica, J. M.; Billin, A.; Blobel, G. A.; Mackay, J. P. Structural Basis and Specificity of Acetylated Transcription Factor GATA1 Recognition by BET Family Bromodomain Protein Brd3∇. *Mol. Cell. Biol.* **2011**, *31*, 2632−2640.
- (31) Lamonica, J. M.; Deng, W.; Kadauke, S.; Campbell, A. E.; Gamsjaeger, R.; Wang, H.; Cheng, Y.; Billin, A. N.; Hardison, R. C.; Mackay, J. P.; Blobel, G. A. Bromodomain Protein Brd3 Associates with Acetylated GATA1 to Promote Its Chromatin Occupancy at Erythroid Target Genes. *Proc. Natl. Acad. Sci. U. S. A.* **2011**, *108*, E159–E168.
- (32) Yang, Z.; Yik, J. H. N.; Chen, R.; He, N.; Jang, M. K.; Ozato, K.; Zhou, Q. Recruitment of P-TEFb for Stimulation of Transcriptional Elongation by the Bromodomain Protein Brd4. *Mol. Cell* **2005**, *19*, 535–545.
- (33) Jang, M. K.; Mochizuki, K.; Zhou, M.; Jeong, H.-S.; Brady, J. N.; Ozato, K. The Bromodomain Protein Brd4 Is a Positive Regulatory

- Component of P-TEFb and Stimulates RNA Polymerase II-Dependent Transcription. *Mol. Cell* **2005**, *19*, 523–534.
- (34) Matzuk, M. M.; McKeown, M. R.; Filippakopoulos, P.; Li, Q.; Ma, L.; Agno, J. E.; Lemieux, M. E.; Picaud, S.; Yu, R. N.; Qi, J.; Knapp, S.; Bradner, J. E. Small-Molecule Inhibition of BRDT for Male Contraception. *Cell* **2012**, *150*, *673*–*684*.
- (35) Gaucher, J.; Boussouar, F.; Montellier, E.; Curtet, S.; Buchou, T.; Bertrand, S.; Hery, P.; Jounier, S.; Depaux, A.; Vitte, A.-L.; Guardiola, P.; Pernet, K.; Debernardi, A.; Lopez, F.; Holota, H.; Imbert, J.; Wolgemuth, D. J.; Gérard, M.; Rousseaux, S.; Khochbin, S. Bromodomain-Dependent Stage-Specific Male Genome Programming by Brdt. *EMBO J.* **2012**, *31*, 3809–3820.
- (36) Berkovits, B. D.; Wolgemuth, D. J. The First Bromodomain of the Testis-Specific Double Bromodomain Protein Brdt Is Required for Chromocenter Organization That Is Modulated by Genetic Background. *Dev. Biol.* **2011**, *360*, 358–368.
- (37) Cheung, K. L.; Zhang, F.; Jaganathan, A.; Sharma, R.; Zhang, Q.; Konuma, T.; Shen, T.; Lee, J.-Y.; Ren, C.; Chen, C.-H.; Lu, G.; Olson, M. R.; Zhang, W.; Kaplan, M. H.; Littman, D. R.; Walsh, M. J.; Xiong, H.; Zeng, L.; Zhou, M.-M. Distinct Roles of Brd2 and Brd4 in Potentiating the Transcriptional Program for Th17 Cell Differentiation. *Mol. Cell* 2017, 65, 1068–1080.e5.
- (38) Gilan, O.; Rioja, I.; Knezevic, K.; Bell, M. J.; Yeung, M. M.; Harker, N. R.; Lam, E. Y. N.; Chung, C.; Bamborough, P.; Petretich, M.; Urh, M.; Atkinson, S. J.; Bassil, A. K.; Roberts, E. J.; Vassiliadis, D.; Burr, M. L.; Preston, A. G. S.; Wellaway, C.; Werner, T.; Gray, J. R.; Michon, A.-M.; Gobbetti, T.; Kumar, V.; Soden, P. E.; Haynes, A.; Vappiani, J.; Tough, D. F.; Taylor, S.; Dawson, S.-J.; Bantscheff, M.; Lindon, M.; Drewes, G.; Demont, E. H.; Daniels, D. L.; Grandi, P.; Prinjha, R. K.; Dawson, M. A. Selective targeting of BD1 and BD2 of the BET proteins in cancer and immunoinflammation. *Science* 2020, 368, 387–394.
- (39) Xu, Y.-M.; Liu, M. X.; Grunow, N.; Wijeratne, E. M. K.; Paine-Murrieta, G.; Felder, S.; Kris, R. M.; Gunatilaka, A. A. L. Discovery of Potent  $17\beta$ -Hydroxywithanolides for Castration-Resistant Prostate Cancer by High-Throughput Screening of a Natural Products Library for Androgen-Induced Gene Expression Inhibitors. *J. Med. Chem.* **2015**, *58*, *6984*–*6993*.
- (40) Tewary, P.; Brooks, A. D.; Xu, Y.-M.; Wijeratne, E. M. K.; Babyak, A. L.; Back, T. C.; Chari, R.; Evans, C. N.; Henrich, C. J.; Meyer, T. J.; Edmondson, E. F.; de Aquino, M. T. P.; Kanagasabai, T.; Shanker, A.; Gunatilaka, A. A. L.; Sayers, T. J. Small-Molecule Natural Product Physachenolide C Potentiates Immunotherapy Efficacy by Targeting BET Proteins. *Cancer Res.* **2021**, *81*, 3374.
- (41) Roberts, J. M.; Bradner, J. E. A Bead-Based Proximity Assay for BRD4 Ligand Discovery. *Curr. Protoc. Chem. Biol.* **2015**, *7*, 263–278.
- (42) Gaudet, E. A.; Huang, K.-S.; Zhang, Y.; Huang, W.; Mark, D.; Sportsman, J. R. A Homogeneous Fluorescence Polarization Assay Adaptable for a Range of Protein Serine/Threonine and Tyrosine Kinases. J. Biomol. Screen. 2003, 8, 164–175.
- (43) Xu, Y.-M.; Wijeratne, E. M. K.; Babyak, A. L.; Marks, H. R.; Brooks, A. D.; Tewary, P.; Xuan, L.-J.; Wang, W.-Q.; Sayers, T. J.; Gunatilaka, A. A. L. Withanolides from Aeroponically Grown Physalis Peruviana and Their Selective Cytotoxicity to Prostate Cancer and Renal Carcinoma Cells. J. Nat. Prod. 2017, 80, 1981–1991.
- (44) Xu, Y.-M.; Wijeratne, E. M. K.; Brooks, A. D.; Tewary, P.; Xuan, L.-J.; Wang, W.-Q.; Sayers, T. J.; Gunatilaka, A. A. L. Cytotoxic and Other Withanolides from Aeroponically Grown Physalis Philadelphica. *Phytochemistry* **2018**, *152*, 174–181.
- (45) Xu, Y.-M.; Brooks, A. D.; Wijeratne, E. M. K.; Henrich, C. J.; Tewary, P.; Sayers, T. J.; Gunatilaka, A. A. L.  $17\beta$ -Hydroxywithanolides as Sensitizers of Renal Carcinoma Cells to Tumor Necrosis Factor- $\alpha$  Related Apoptosis Inducing Ligand (TRAIL) Mediated Apoptosis: Structure—Activity Relationships. *J. Med. Chem.* **2017**, *60*, 3039–3051. (46) Xu, Y.; Bunting, D. P.; Liu, M. X.; Bandaranayake, H. A.; Cunatilaka, A. A. J. 17 $\beta$  Hydroxy, 18 Acetayaryithanolides, from
- (46) Xu, Y.; Bunting, D. P.; Liu, M. X.; Bandaranayake, H. A.; Gunatilaka, A. A. L.  $17\beta$ -Hydroxy-18-Acetoxywithanolides from Aeroponically Grown *Physalis Crassifolia* and Their Potent and Selective Cytotoxicity for Prostate Cancer Cells. *J. Nat. Prod.* **2016**, 79, 821–830.

- (47) Xu, Y.-m.; Marron, M. T.; Seddon, E.; McLaughlin, S. P.; Ray, D. T.; Whitesell, L.; Gunatilaka, A. A. L. 2,3-Dihydrowithaferin A-3beta-O-Sulfate, a New Potential Prodrug of Withaferin A from Aeroponically Grown Withania Somnifera. *Bioorg. Med. Chem.* **2009**, *17*, 2210–2214.
- (48) Kregel, S.; Malik, R.; Asangani, I. A.; Wilder-Romans, K.; Rajendiran, T.; Xiao, L.; Vo, J. N.; Soni, T.; Cieslik, M.; Fernadez-Salas, E.; Zhou, B.; Cao, X.; Speers, C.; Wang, S.; Chinnaiyan, A. M. Functional and Mechanistic Interrogation of BET Bromodomain Degraders for the Treatment of Metastatic Castration-Resistant Prostate Cancer. Clin. Cancer Res. 2019, 25, 4038–4048.
- (49) Chen, L.-X.; He, H.; Qiu, F. Natural Withanolides: An Overview. *Nat. Prod. Rep.* **2011**, 28, 705.
- (50) Machin, R. P.; Veleiro, A. S.; Nicotra, V. E.; Oberti, J. C.; Padrón, J. M. Antiproliferative Activity of Withanolides against Human Breast Cancer Cell Lines. *J. Nat. Prod.* **2010**, *73*, 966–968.
- (51) Liu, Z.; Wang, P.; Chen, H.; Wold, E. A.; Tian, B.; Brasier, A. R.; Zhou, J. Drug Discovery Targeting Bromodomain-Containing Protein 4. *J. Med. Chem.* **2017**, *60*, 4533–4558.
- (52) Bolden, J. E.; Tasdemir, N.; Dow, L. E.; van Es, J. H.; Wilkinson, J. E.; Zhao, Z.; Clevers, H.; Lowe, S. W. Inducible in Vivo Silencing of Brd4 Identifies Potential Toxicities of Sustained BET Protein Inhibition. *Cell Rep.* **2014**, *8*, 1919–1929.
- (53) Tang, P.; Zhang, J.; Liu, J.; Chiang, C.-M.; Ouyang, L. Targeting Bromodomain and Extraterminal Proteins for Drug Discovery: From Current Progress to Technological Development. *J. Med. Chem.* **2021**, *64*, 2419–2435.
- (54) Wu, S.-Y.; Lee, A.-Y.; Lai, H.-T.; Zhang, H.; Chiang, C.-M. Phospho Switch Triggers Brd4 Chromatin Binding and Activator Recruitment for Gene-Specific Targeting. *Mol. Cell* **2013**, *49*, 843–857.
- (55) Wu, S.-Y.; Lee, C.-F.; Lai, H.-T.; Yu, C.-T.; Lee, J.-E.; Zuo, H.; Tsai, S. Y.; Tsai, M.-J.; Ge, K.; Wan, Y.; Chiang, C.-M. Opposing Functions of BRD4 Isoforms in Breast Cancer. *Mol. Cell* **2020**, 78, 1114–1132.e10.
- (56) Wu, S.-Y.; Nin, D. S.; Lee, A.-Y.; Simanski, S.; Kodadek, T.; Chiang, C.-M. BRD4 Phosphorylation Regulates HPV E2-Mediated Viral Transcription, Origin Replication, and Cellular MMP-9 Expression. *Cell Rep.* **2016**, *16*, 1733–1748.
- (57) Sabò, A.; Amati, B. BRD4 and MYC-Clarifying Regulatory Specificity. *Science* **2018**, *360*, 713–714.
- (58) Devaiah, B. N.; Mu, J.; Akman, B.; Uppal, S.; Weissman, J. D.; Cheng, D.; Baranello, L.; Nie, Z.; Levens, D.; Singer, D. S. MYC Protein Stability Is Negatively Regulated by BRD4. *Proc. Natl. Acad. Sci. U. S. A.* **2020**, *117*, 13457–13467.
- (59) Liu, Z.; Tian, B.; Chen, H.; Wang, P.; Brasier, A. R.; Zhou, J. Discovery of Potent and Selective BRD4 Inhibitors Capable of Blocking TLR3-Induced Acute Airway Inflammation. *Eur. J. Med. Chem.* **2018**, *151*, 450–461.
- (60) Lu, J.; Qian, Y.; Altieri, M.; Dong, H.; Wang, J.; Raina, K.; Hines, J.; Winkler, J. D.; Crew, A. P.; Coleman, K.; Crews, C. M. Hijacking the E3 Ubiquitin Ligase Cereblon to Efficiently Target BRD4. *Chem. Biol.* **2015**, 22, 755–763.
- (61) Sayers, T. J.; Tewary, P.; Gunatilaka, L.; Brooks, A. D.; Wijeratne, E. M. K.; Xu, Y. 17-Beta-Hydroxywithanolides and Use Thereof in Treating Cancer. WO2019173499A1, September 12, 2019.
- (62) Blee, A. M.; Liu, S.; Wang, L.; Huang, H. BET Bromodomain-Mediated Interaction between ERG and BRD4 Promotes Prostate Cancer Cell Invasion. *Oncotarget* **2016**, *7*, 38319–38332.
- (63) Zuber, V.; Bettella, F.; Witoelar, A.; PRACTICAL Consortium; CRUK GWAS; BCAC Consortium; TRICL Consortium; Andreassen, O. A.; Mills, I. G.; Urbanucci, A. Bromodomain Protein 4 Discriminates Tissue-Specific Super-Enhancers Containing Disease-Specific Susceptibility Loci in Prostate and Breast Cancer. *BMC Genomics* **2017**, *18*, 270.
- (64) Tan, Y.; Wang, L.; Du, Y.; Liu, X.; Chen, Z.; Weng, X.; Guo, J.; Chen, H.; Wang, M.; Wang, X. Inhibition of BRD4 Suppresses Tumor Growth in Prostate Cancer via the Enhancement of FOXO1 Expression. *Int. J. Oncol.* **2018**, *53*, 2503–2517.
- (65) Jin, X.; Yan, Y.; Wang, D.; Ding, D.; Ma, T.; Ye, Z.; Jimenez, R.; Wang, L.; Wu, H.; Huang, H. DUB3 Promotes BET Inhibitor

- Resistance and Cancer Progression by Deubiquitinating BRD4. *Mol. Cell* **2018**, *71*, 592–605.e4.
- (66) Dong, G.; Ding, Y.; He, S.; Sheng, C. Molecular Glues for Targeted Protein Degradation: From Serendipity to Rational Discovery. *J. Med. Chem.* **2021**, *64*, 10606–10620.
- (67) Schreiber, S. L. The Rise of Molecular Glues. *Cell* **2021**, 184, 3–9.
- (68) Edmondson, S. D.; Yang, B.; Fallan, C. Proteolysis Targeting Chimeras (PROTACs) in 'beyond Rule-of-Five' Chemical Space: Recent Progress and Future Challenges. *Bioorg. Med. Chem. Lett.* **2019**, 29, 1555–1564.
- (69) Chamberlain, P. P.; Hamann, L. G. Development of Targeted Protein Degradation Therapeutics. *Nat. Chem. Biol.* **2019**, *15*, 937–944.
- (70) Marley, J.; Lu, M.; Bracken, C. A Method for Efficient Isotopic Labeling of Recombinant Proteins. *J. Biomol.* **2001**, *20*, 71–75.
- (71) Grzesiek, S.; Bax, A. Correlating Backbone Amide and Side Chain Resonances in Larger Proteins by Multiple Relayed Triple Resonance NMR. *J. Am. Chem. Soc.* **1992**, *114*, 6291–6293.
- (72) Muhandiram, D. R.; Kay, L. E. Gradient-Enhanced Triple-Resonance Three-Dimensional NMR Experiments with Improved Sensitivity. *J. Magn. Reson. B* **1994**, *103*, 203–216.
- (73) Lee, W.; Tonelli, M.; Markley, J. L. NMRFAM-SPARKY: Enhanced Software for Biomolecular NMR Spectroscopy. *Bioinforma*. **2015**, *31*, 1325–1327.
- (74) Lee, W.; Bahrami, A.; Dashti, H. T.; Eghbalnia, H. R.; Tonelli, M.; Westler, W. M.; Markley, J. L. I-PINE Web Server: An Integrative Probabilistic NMR Assignment System for Proteins. *J. Biomol. NMR* **2019**, 73, 213–222.
- (75) Kabsch, W. Processing of X-Ray Snapshots from Crystals in Random Orientations. *Acta Crystallogr. D Biol. Crystallogr.* **2014**, 70, 2204–2216.
- (76) Winn, M. D.; Ballard, C. C.; Cowtan, K. D.; Dodson, E. J.; Emsley, P.; Evans, P. R.; Keegan, R. M.; Krissinel, E. B.; Leslie, A. G. W.; McCoy, A.; McNicholas, S. J.; Murshudov, G. N.; Pannu, N. S.; Potterton, E. A.; Powell, H. R.; Read, R. J.; Vagin, A.; Wilson, K. S. Overview of the CCP 4 Suite and Current Developments. Acta Crystallogr. D Biol. Crystallogr. 2011, 67, 235–242.
- (77) McCoy, A. J. Solving Structures of Protein Complexes by Molecular Replacement with Phaser. *Acta Crystallogr. D Biol. Crystallogr.* **2007**, *63*, 32–41.
- (78) Fromme, R.; Katiliene, Z.; Giomarelli, B.; Bogani, F.; Mc Mahon, J.; Mori, T.; Fromme, P.; Ghirlanda, G. A Monovalent Mutant of Cyanovirin-N Provides Insight into the Role of Multiple Interactions with Gp120 for Antiviral Activity. *Biochemistry* **2007**, *46*, 9199–9207.
- (79) Fromme, R.; Katiliene, Z.; Fromme, P.; Ghirlanda, G. Conformational gating of dimannose binding to the antiviral protein cyanovirin revealed from the crystal structure at 1.35 Å resolution. *PROTEIN Sci.* **2008**, *17*, 939–944.
- (80) Emsley, P.; Lohkamp, B.; Scott, W. G.; Cowtan, K. Features and Development of *Coot. Acta Crystallogr. D Biol. Crystallogr.* **2010**, *66*, 486–501.
- (81) Adams, P. D.; Afonine, P. V.; Bunkóczi, G.; Chen, V. B.; Davis, I. W.; Echols, N.; Headd, J. J.; Hung, L.-W.; Kapral, G. J.; Grosse-Kunstleve, R. W.; McCoy, A. J.; Moriarty, N. W.; Oeffner, R.; Read, R. J.; Richardson, D. C.; Richardson, J. S.; Terwilliger, T. C.; Zwart, P. H. PHENIX: A Comprehensive Python-Based System for Macromolecular Structure Solution. *Acta Crystallogr. D Biol. Crystallogr.* 2010, 66, 213–221.
- (82) McPhillips, T. M.; McPhillips, S. E.; Chiu, H.-J.; Cohen, A. E.; Deacon, A. M.; Ellis, P. J.; Garman, E.; Gonzalez, A.; Sauter, N. K.; Phizackerley, R. P.; Soltis, S. M.; Kuhn, P. Blu-Ice and the Distributed Control System: Software for Data Acquisition and Instrument Control at Macromolecular Crystallography Beamlines. *J. Synchrotron Radiat.* **2002**, *9*, 401–406.
- (83) Kabsch, W. Integration, Scaling, Space-Group Assignment and Post-Refinement. *Acta Crystallogr. D Biol. Crystallogr.* **2010**, *66*, 133–144.

- (84) Kabsch, W. XDS. Acta Crystallogr. D Biol. Crystallogr. 2010, 66, 125–132.
- (85) Evans, P. Scaling and Assessment of Data Quality. *Acta Crystallogr. D Biol. Crystallogr.* **2006**, 62, 72–82.
- (86) Evans, P. Data Reduction; Proceedings of CCP4 Study Weekend; 1993; Vol. On Data Collection&Processing.
- (87) McCoy, A. J.; Grosse-Kunstleve, R. W.; Adams, P. D.; Winn, M. D.; Storoni, L. C.; Read, R. J. Phaser Crystallographic Software. *J. Appl. Crystallogr.* **2007**, *40*, 658–674.
- (88) Adams, P. D.; Grosse-Kunstleve, R. W.; Hung, L. W.; Ioerger, T. R.; McCoy, A. J.; Moriarty, N. W.; Read, R. J.; Sacchettini, J. C.; Sauter, N. K.; Terwilliger, T. C. PHENIX: Building New Software for Automated Crystallographic Structure Determination. *Acta Crystallogr. D Biol. Crystallogr.* **2002**, *58*, 1948–1954.
- (89) Emsley, P.; Cowtan, K. Coot: Model-Building Tools for Molecular Graphics. *Acta Crystallogr. D Biol. Crystallogr.* **2004**, *60*, 2126–2132.
- (90) Moriarty, N. W.; Grosse-Kunstleve, R. W.; Adams, P. D. Electronic Ligand Builder and Optimization Workbench (ELBOW): A Tool for Ligand Coordinate and Restraint Generation. *Acta Crystallogr. D Biol. Crystallogr.* **2009**, *65*, 1074–1080.
- (91) Grosse-Kunstleve, R. W.; Terwilliger, T. C.; Sauter, N. K.; Adams, P. D. Automatic Fortran to C++ Conversion with FABLE. *Source Code Biol. Med.* **2012**, *7*, 5.
- (92) Headd, J. J.; Echols, N.; Afonine, P. V.; Grosse-Kunstleve, R. W.; Chen, V. B.; Moriarty, N. W.; Richardson, D. C.; Richardson, J. S.; Adams, P. D. Use of Knowledge-Based Restraints in Phenix. Refine to Improve Macromolecular Refinement at Low Resolution. *Acta Crystallogr. D Biol. Crystallogr.* **2012**, *68*, 381–390.
- (93) Afonine, P. V.; Grosse-Kunstleve, R. W.; Adams, P. D.; Urzhumtsev, A. Bulk-Solvent and Overall Scaling Revisited: Faster Calculations, Improved Results. *Acta Crystallogr. D Biol. Crystallogr.* **2013**, *69*, 625–634.